

# Network inference in a stochastic multi-population neural mass model via approximate Bayesian computation

Susanne Ditlevsen\*, Massimiliano Tamborrino†, Irene Tubikanec‡

## Abstract

The aim of this article is to infer the connectivity structures of brain regions before and during epileptic seizure. Our contributions are fourfold. First, we propose a  $6N$ -dimensional stochastic differential equation for modelling the activity of  $N$  coupled populations of neurons in the brain. This model further develops the (single population) stochastic Jansen and Rit neural mass model, which describes human electroencephalography (EEG) rhythms, in particular signals with epileptic activity. Second, we construct a reliable and efficient numerical scheme for the model simulation, extending a splitting procedure proposed for one neural population. Third, we propose an adapted Sequential Monte Carlo Approximate Bayesian Computation algorithm for simulation-based inference of both the relevant real-valued model parameters as well as the  $\{0, 1\}$ -valued network parameters, the latter describing the coupling directions among the  $N$  modelled neural populations. Fourth, after illustrating and validating the proposed statistical approach on different types of simulated data, we apply it to a set of multi-channel EEG data recorded before and during an epileptic seizure. The real data experiments suggest, for example, a larger activation in each neural population and a stronger connectivity on the left brain hemisphere during seizure.

## Keywords

Jansen and Rit neural mass model, Stochastic Hamiltonian systems, Splitting methods, Approximate Bayesian computation, Simulation-based inference, EEG data

## AMS subject classifications

60H10, 60H35, 65C30

## Authorship contribution statement

S.D., M.T. and I.T. designed the study. I.T. performed the analysis, wrote the code, and produced all figures. I.T. wrote the first draft. S.D., M.T. and I.T. discussed the results and implications, commented on the manuscript at all stages, edited the text and approved the final version.

## Acknowledgements

S.D. was supported by the Novo Nordisk Foundation NNF20OC0062958 and the Independent Research Fund Denmark | Natural Sciences 9040-00215B. A part of this paper was written while I.T. was member of the Institute of Stochastics, Johannes Kepler University Linz, 4040 Linz, Austria. During this time, I.T. was supported by the Austrian Science Fund (FWF): W1214-N15, project DK14. The authors are also grateful for the generous mobility funding provided by the University of Klagenfurt.

\*Department of Mathematical Sciences, University of Copenhagen (susanne@math.ku.dk)

†Department of Statistics, University of Warwick (massimiliano.tamborrino@warwick.ac.uk)

‡Department of Statistics, University of Klagenfurt (irene.tubikanec@aau.at)

# 1 Introduction

Estimating the connectivity in a network of units is important in a vast variety of applications, ranging from biology over climate to finance, physics, sociology and other fields. This is a statistically challenging task, as these interacting units typically follow some complex underlying stochastic dynamics, which may be only partially observed. Moreover, the detection of directed connections and the distinction from spurious ones is particularly difficult. This article is motivated by neuroscience, where the study of neural activity and the underlying connectivity between brain regions is essential for understanding brain function and its implications in various neurological conditions. In particular, we are interested in inferring the connectivity structure of the brain before and during epileptic seizure, a critical area of study for understanding and managing epilepsy. Electroencephalography (EEG) is a widely used technique to measure and analyze brain activity, providing insights into the complex dynamics of the brain. Here, we aim at estimating the directed connections between  $N$  coupled neural populations whose activity corresponds to the simultaneous measurements from  $N$  electrodes in the EEG recordings, one per population.

In this article, each neural population is modelled with a stochastic version of the Jansen and Rit neural mass model (JR-NMM) originally proposed in [18]. This model has shown useful for reproducing human EEG rhythms, including those associated with epileptic activity. The original JR-NMM is a 6-dimensional system of ordinary differential equations and describes the average activity of one neural population, corresponding to the measured activity of one electrode in EEG recordings. The model includes a term representing noisy extrinsic input from the neighborhood or more distant regions. As this term can be interpreted as a stochastic process, the solution of the dynamical system is a stochastic process as well, inheriting the analytical properties of this stochastic input function. Therefore, the model was reformulated as a stochastic differential equation (SDE) in [1], and proved to be geometrically ergodic, a property guaranteeing that the distribution of the solution converges to a unique limit distribution, exponentially fast and for any initial value. This has two important statistical implications: First, the choice of the (unknown) initial value is negligible, since its impact on the distribution of the process decreases exponentially fast. Second, quantities related to the distribution of the process can be estimated from a (sufficiently long) single path, instead of requiring many repeated path simulations. While the original JR-NMM [18] has been extended to model  $N$  coupled neural populations in [42], no such extension has been proposed for the SDE version [1] of this model. We fill in this gap by proposing a  $6N$ -dimensional SDE model accounting for directed connections between  $N$  neural populations (*first contribution*). In contrast to [42], our model contains  $\{0, 1\}$ -valued coupling direction parameters, describing the underlying network structure that we aim to infer from EEG data.

As neither the underlying transition density nor exact simulation schemes are available for the  $6N$ -dimensional SDE model, a suitable numerical approximation is required. The commonly applied Euler-Maruyama discretisation is not suitable for this SDE, as it has been shown to fail in preserving crucial structural properties for the single population model, such as the dynamics of the modelled neural oscillations [1, 8]. The interested reader is also referred to [7, 10, 11, 20, 37], where similar issues of the Euler-Maruyama method applied to oscillatory SDE models are reported. Consequently, when embedded into a statistical inference procedure, this standard numerical scheme may yield wrong estimation results, make the inference algorithm computationally infeasible or lead to ill-conditioned estimation methods [8, 14, 29]. Therefore, to obtain a reliable and efficient numerical simulation method, we further develop the structure-preserving splitting procedure proposed in [1] for  $N = 1$  population to our  $N$ -population SDE model (*second contribution*). In contrast to the Euler-Maruyama scheme, which is based on truncating a stochastic Taylor series, the idea behind the splitting approach is to divide the unsolvable equation into solvable subequations, and to compose their solutions in a proper way [5, 24]. The constructed splitting scheme for the stochastic  $N$ -population neural mass model is based on a Hamiltonian type re-formulation of the SDE and successfully handles multiple interacting components, allowing to accurately simulate the complex dynamics of coupled neural populations.

As a next step, we aim to estimate the  $\{0, 1\}$ -valued coupling direction parameters between the  $N$  neural populations, as well as relevant real-valued model parameters of the  $6N$ -dimensional

SDE from  $N$  simultaneously recorded EEG signals. This is particularly challenging, since this SDE falls into the class of hypoelliptic models [14, 21, 25, 29] and is only partially observed via  $N$  one-dimensional linear functions of a subset of the  $6N$  model components. These issues, combined with the lack of a tractable underlying likelihood, make this problem naturally suitable for likelihood-free inference approaches. We focus on the simulation-based Approximate Bayesian Computation (ABC) method [34], which has become one of the leading tools for parameter estimation in complex mathematical models in the last decades. The idea behind the classical acceptance-rejection ABC algorithm is to: (a) sample a parameter candidate from a prior distribution; (b) simulate a dataset conditioned on this value; (c) keep the candidate as a sample from the desired approximate posterior if the distance between the summary statistics of the simulated and observed datasets is smaller than some threshold level [4, 23, 34]. This basic algorithm is computationally expensive, because parameter candidates are sampled from the prior distribution throughout, whose mass typically concentrates in regions “far away” from those of the posterior distribution, leading to low acceptance rates and high computational costs. To tackle this, here we consider the Sequential Monte Carlo (SMC) ABC approach, which represents the state-of-the-art sampler within ABC. This sequential algorithm relies on targeted proposal samplers (constructed across iterations) that efficiently avoid improbable parameter regions, yielding intermediate approximate posterior distributions that move towards the desired posterior during several iterations [3, 13, 35]. In particular, we propose an adapted SMC-ABC algorithm to infer both the  $\{0, 1\}$ -valued network parameters and the real-valued model parameters (*third contribution*). The algorithm builds upon the work of [8] for Hamiltonian-type SDEs observed via univariate time series, further developing it at the following three levels. First, we rely on the numerical splitting scheme for synthetic data generation from the  $6N$ -dimensional SDE. Second, we construct effective summary statistics by mapping the  $N$ -dimensional time series to their estimated  $N$  marginal densities and spectral densities, as well as to their estimated cross-spectral densities and cross-correlation functions to account for possible dependencies among the populations. Third and foremost, to handle the high-dimensional parameter space and the presence of  $\{0, 1\}$ -valued parameters, we consider two independent kernels for the SMC-ABC proposal, one Gaussian for the real-valued and one Bernoulli for the  $\{0, 1\}$ -valued parameters. By estimating the latter, we uncover the directed connectivity structure of the neural populations, enabling the identification of the intricate network connections within brain regions.

After validating the performance of the proposed statistical approach on different types of simulated data, we apply it on real multi-channel EEG data measured before and during epileptic seizure (*fourth contribution*). We successfully obtain unimodal posteriors of a relatively large number of continuous model parameters and a clear network estimate during seizure. Comparing this network with that obtained based on the EEG recordings before seizure, we observe, e.g., a stronger connectivity on the left brain hemisphere during seizure.

The proposed algorithm, along with the choice of its key ingredients, holds promise beyond the specific application, as it can be used for other coupled ergodic SDE models, provided that a reliable numerical simulation method can be derived. This flexibility broadens the scope of our work, offering a potential avenue for parameter and network estimation in various complex stochastic systems involving coupled units.

The paper is organised as follows. In Section 2, we introduce the model. In Section 3, we construct the numerical splitting method. In Section 4, we detail the proposed adapted SMC-ABC algorithm for network inference. In Section 5, we illustrate its performance on simulated data. In Section 6, we apply our method to real EEG data with epileptic activity. Conclusions and discussion are reported in Section 7. Sample code is available at <https://github.com/IreneTubikanec/networkABC>.

## 2 Multi-population stochastic Jansen and Rit neural mass model

We first present the stochastic JR-NMM of one neural population [1]. We then extend it to a system of multiple coupled neural populations, following the strategies proposed in [19, 42]. Finally, inspired by [1], we derive the corresponding Hamiltonian type formulation of the multi-population model.

**Notation** We denote by  $0_d$  the  $d$ -dimensional zero vector, by  $\mathbb{O}_d$  the  $d \times d$ -dimensional zero matrix, by  $\mathbb{I}_d$  the  $d \times d$ -dimensional identity matrix, and by  $\text{diag}[a_1, \dots, a_d]$  a  $d \times d$ -dimensional diagonal matrix with diagonal entries  $a_1, \dots, a_d$ . The transpose is denoted by  $^\top$  and the Euclidean norm by  $\|\cdot\|$ . We sometimes omit the time index of a stochastic process and use, e.g.,  $(X(t))_{t \in [0, T]}$  and  $X$  interchangeably.

## 2.1 Modelling one neural population

Let  $[0, T]$ , with  $T > 0$ , be the time interval of interest. Let  $(\Omega, \mathcal{F}, \mathbb{P})$  be a complete probability space with a complete and right-continuous filtration  $(\mathcal{F}(t))_{t \in [0, T]}$ , and let  $(W_i(t))_{t \in [0, T]}$ ,  $i = 4, 5, 6$ , be independent Wiener processes on  $(\Omega, \mathcal{F}, \mathbb{P})$  and adapted to  $(\mathcal{F}(t))_{t \in [0, T]}$ .

Let  $X_i$ ,  $i = 1, 2, 3$ , model the average postsynaptic potentials of three groups of neurons, i.e., the main neurons, excitatory interneurons and inhibitory interneurons, respectively. Define the sigmoid function  $\text{sig}: \mathbb{R} \rightarrow [0, \nu_{\max}]$ , with  $\nu_{\max} > 0$ , by

$$\text{sig}(x) := \frac{\nu_{\max}}{1 + e^{\gamma(v_0 - x)}},$$

where  $x$  is a potential,  $\nu_{\max}$  describes the maximum firing rate of the neural population,  $v_0 \in \mathbb{R}$  is the potential value for which 50% of the maximum firing rate is attained and  $\gamma > 0$  is proportional to the slope of the sigmoid function at  $v_0$ . The sigmoid function is used to transform the average membrane potential of a neural subpopulation into an average firing rate. The stochastic version of the JR-NMM [1] is given by

$$\begin{aligned} dX_1(t) &= X_4(t)dt \\ dX_2(t) &= X_5(t)dt \\ dX_3(t) &= X_6(t)dt \\ dX_4(t) &= [Aa(\text{sig}(X_2(t) - X_3(t))) - 2aX_4(t) - a^2X_1(t)] dt + \bar{\epsilon}dW_4(t) \\ dX_5(t) &= [Aa(\mu + C_2\text{sig}(C_1X_1(t))) - 2aX_5(t) - a^2X_2(t)] dt + \sigma dW_5(t) \\ dX_6(t) &= [BbC_4\text{sig}(C_3X_1(t)) - 2bX_6(t) - b^2X_3(t)] dt + \tilde{\epsilon}dW_6(t), \end{aligned} \tag{1}$$

with  $\mathcal{F}(0)$ -measurable initial value  $X_0 = (X_1(0), \dots, X_6(0))^\top$  which is independent of  $W = (W_4, W_5, W_6)^\top$  and satisfies  $\mathbb{E}[\|X_0\|^2] < \infty$ . The meaning and typical values of the model parameters  $A, B, a, b, C_1, C_2, C_3, C_4, \nu_{\max}, \gamma$  and  $v_0$  are reported in Table 1 (see also [1, 18, 42]). The parameters  $\mu$  and  $\sigma$  scale the deterministic and stochastic input, respectively, coming from neighboring regions in the brain. Together with the Wiener process  $W_5$ , they replace the stochastic input function of the original model. While usually  $\sigma \gg 1$ , weak noise acts on the components  $X_4$  and  $X_6$  with noise intensities  $\bar{\epsilon}, \tilde{\epsilon} \ll \sigma$ . Throughout, we set  $\epsilon = \bar{\epsilon} = \tilde{\epsilon} = 1 \text{ s}^{-1}$ , since their role is marginal. See [1] for further details.

The stochastic JR-NMM (1) is an additive noise SDE with globally Lipschitz drift coefficient, and thus has a pathwise unique solution which is adapted to  $(\mathcal{F}(t))_{t \in [0, T]}$  [2, 22]. Moreover, system (1) is hypoelliptic and geometrically ergodic [1]. The 6-dimensional solution  $X = (X_1, X_2, X_3, X_4, X_5, X_6)^\top$  is only partially observed through the difference of two of its coordinates

$$Y(t) := X_2(t) - X_3(t), \quad t \in [0, T]. \tag{2}$$

The process  $Y = (Y(t))_{t \in [0, T]}$  is the observed *output* of the model and describes the average membrane potential of the main neurons as measured with EEG. An illustration of a simulated trace with parameters chosen to produce  $\alpha$ -waves (neural oscillations in the 8–12 Hz frequency band) is provided in Figure 1, Panel A. The model can also produce more complex behaviour, such as brain signals occurring before and during epileptic seizures. This is achieved by increasing the excitation-inhibition-ratio  $A/B$  [42]. In Figure 1 Panel B, regular EEG activity is produced by using  $\mu = 90$ ,  $\sigma = 500$ ,  $A = 3.25$  and the standard values reported in Table 1. Increasing the excitation-inhibition-ratio by increasing  $A$  causes the model to generate sporadic and frequently occurring spikes ( $A = 3.5$  and  $A = 3.6$ ) and rhythmic discharge of spikes ( $A = 4.3$ ), as observed in Panels C-E, respectively.

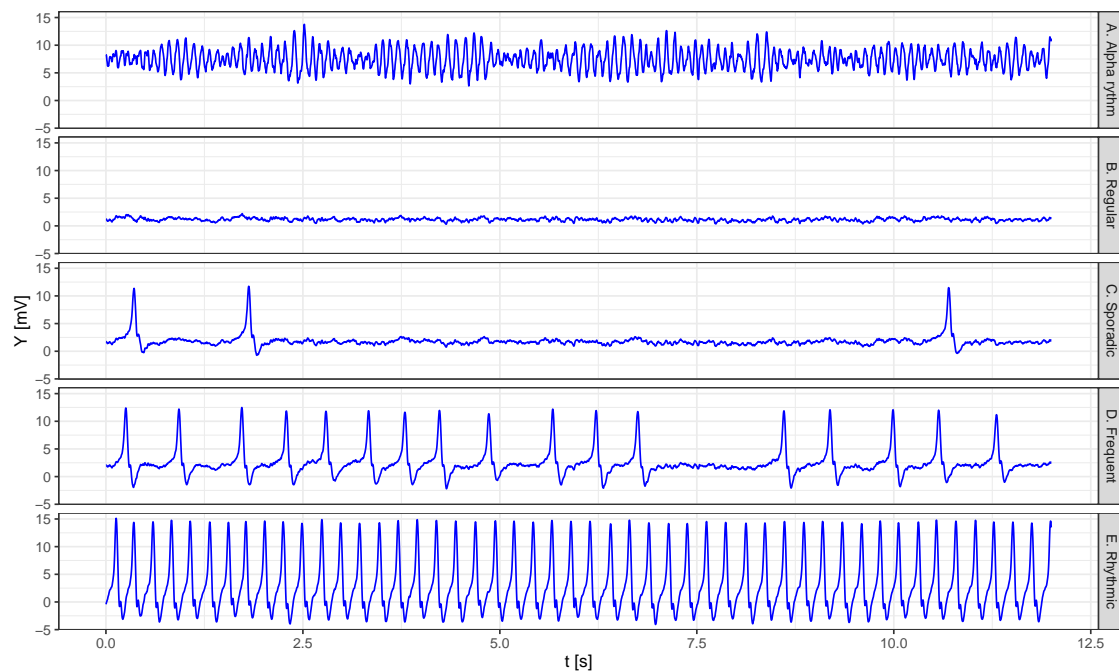


Figure 1: **Traces of one neural population with different types of activity.** Simulated paths of the process  $Y$  in eq. (2) of model (1). Panel A: Trace showing  $\alpha$ -rhythmic activity using the standard values of Table 1,  $A = 3.25, C = 134.263, \mu = 202.547,$  and  $\sigma = 1859.211$  (values taken from [8]). Panels B-E: Traces describing activity occurring during epileptic seizures using the standard values of Table 1,  $\mu = 90, \sigma = 500$  and different values of  $A$ . Panel B: Regular EEG,  $A = 3.25$ . Panel C: Sporadic spikes,  $A = 3.5$ . Panel D: Frequently occurring spikes,  $A = 3.6$ . Panel E: Rhythmic discharge of spikes,  $A = 4.3$ . The signals resemble experimental stereo EEG recordings (cf. Figure 3 in [42]).

Table 1: Standard parameter values for the Jansen and Rit Neural Mass Model [1, 18, 42].

Parameter	Meaning	Standard value
$A$	Average excitatory synaptic gain	3.25 mV
$B$	Average inhibitory synaptic gain	22 mV
$a$	Membrane time constant of excitatory postsynaptic potential	$100 \text{ s}^{-1}$
$b$	Membrane time constant of inhibitory postsynaptic potential	$50 \text{ s}^{-1}$
$C$	Average number of synapses between the subpopulations	135
$C_1, C_2$	Avg. no. of synaptic contacts in the excitatory feedback loop	$C, 0.8 C$
$C_3, C_4$	Avg. no. of synaptic contacts in the inhibitory feedback loop	$0.25 C, 0.25 C$
$\nu_{\max}$	Maximum firing rate (Maximum of the sigmoid function)	$5 \text{ s}^{-1}$
$v_0$	Value for which 50% of the maximum firing rate is attained	6 mV
$\gamma$	Determines the slope of the sigmoid function at $v_0$	$0.56 \text{ mV}^{-1}$

## 2.2 Modelling multiple coupled neural populations

Here, we define the  $6N$ -dimensional SDE describing a system of  $N > 1$  neural populations, where the  $k$ -th population  $X^k = (X_1^k, \dots, X_6^k)$ ,  $k = 1, \dots, N$ , satisfies (1) with suitable index  $k$ , except for the fifth equation, which is instead given by

$$dX_5^k(t) = \left[ A_k a_k \left( \mu_k + C_{2,k} \text{sig}(C_{1,k} X_1^k(t)) + \sum_{j=1, j \neq k}^N \rho_{jk} K_{jk} X_1^j(t) \right) - 2a_k X_5^k(t) - a_k^2 X_2^k(t) \right] dt + \sigma_k dW_5^k(t).$$

In particular, the  $k$ -th population  $X^k$  receives inputs from populations  $j \neq k$ ,  $j = 1, \dots, N$ , through its coordinate  $X_5^k$ , where  $K_{jk} > 0$  model the coupling strengths and  $\rho_{jk} \in \{0, 1\}$  determine whether there is ( $\rho_{jk} = 1$ ) or not ( $\rho_{jk} = 0$ ) a directed coupling from the  $j$ -th to the  $k$ -th population, defining thus the functional network of relations among the neural populations. Since the main pyramidal cells are excitatory and have axons reaching other brain areas, the average action potential  $X_1^j(t)$  of population  $j \neq k$  provides excitatory input to population  $k$ , and thus  $K_{jk} > 0$ . Note that the coupling direction parameters  $\rho_{jk}$  were not considered in the modelling approach discussed in [42].

The  $N$ -dimensional observed *output* is

$$Y(t) := (Y^1(t), \dots, Y^N(t))^\top = (X_2^1(t) - X_3^1(t), \dots, X_2^N(t) - X_3^N(t))^\top, \quad t \in [0, T]. \quad (3)$$

Not only the excitation-inhibition-ratio  $A/B$  is relevant for epileptic behaviour, but also the coupling strengths and directions between neural groups play a crucial role [42]. This is illustrated in Figure 2, where simulated activity of  $N = 4$  neural populations under different coupling regimes is shown. In the left panels, no coupling occurs, i.e., all  $\rho_{jk}$  are set to zero. In the middle and right panels, there is a unidirectional (cascade) coupling structure (illustrated in Figure 3a), i.e.,  $\rho_{12} = \rho_{23} = \rho_{34} = 1$ , for different coupling strengths  $K$ . The activity of a passive site (no epileptic spikes occur without input from other populations) strongly depends on that of an active site (epileptic spikes occur without input from other populations). In Population 1, the excitation-inhibition-ratio is increased by setting  $A_1 = 3.6$  to obtain spiking activity. In the remaining populations, the standard values of Table 1,  $\mu = 90$  and  $\sigma = 500$  are used for each component. When there is no coupling among the populations, no activation of Populations 2–4 occurs (left panels). Introducing coupling and setting the coupling strength parameters to  $K_{12} = K_{23} = K_{34} = 300$  (central panels) leads to a dependence of the activity of Populations 2–4 on that of Population 1. When the coupling is strong enough ( $K_{12} = K_{23} = K_{34} = 500$ , right panels), rhythmic synchronization occurs. A similar behaviour for two populations has also been observed for the original JR-NMM (cf. Figure 6 in [42]).

## 2.3 Formulation as a stochastic Hamiltonian type system

The multi-population JR-NMM can be formulated as a damped stochastic Hamiltonian system with non-linear displacement, similarly to [1] for  $N = 1$ . This allows for a more compact formulation and constitutes the basis for the derivation of the numerical method in Section 3.

First, let us decompose the  $k$ -th process as  $X^k := (Q^k, P^k)^\top$  with 3-dimensional components  $Q^k = (X_1^k, X_2^k, X_3^k)^\top$  and  $P^k = (X_4^k, X_5^k, X_6^k)^\top$ . Then, let us denote the 3-dimensional Wiener process in the  $k$ -th population by  $W^k = (W_4^k, W_5^k, W_6^k)^\top$  and the corresponding  $3 \times 3$ -dimensional diffusion matrix by  $\Sigma_k = \text{diag}[\epsilon_k, \sigma_k, \epsilon_k]$ . The Hamiltonian type formulation of the  $k$ -th population is

$$d \begin{pmatrix} Q^k(t) \\ P^k(t) \end{pmatrix} = \begin{pmatrix} \nabla_P H_k(Q^k(t), P^k(t)) \\ -\nabla_Q H_k(Q^k(t), P^k(t)) - 2\Gamma_k P^k(t) + G_k(Q(t)) \end{pmatrix} dt + \begin{pmatrix} \mathbb{O}_3 \\ \Sigma_k \end{pmatrix} dW^k(t). \quad (4)$$

System (4) consists of a *Hamiltonian part* defined by the Hamiltonian function  $H_k : \mathbb{R}^6 \rightarrow \mathbb{R}_0^+$  given by

$$H_k(Q^k, P^k) := \frac{1}{2} \left( \|P^k\|^2 + \|\Gamma_k Q^k\|^2 \right),$$

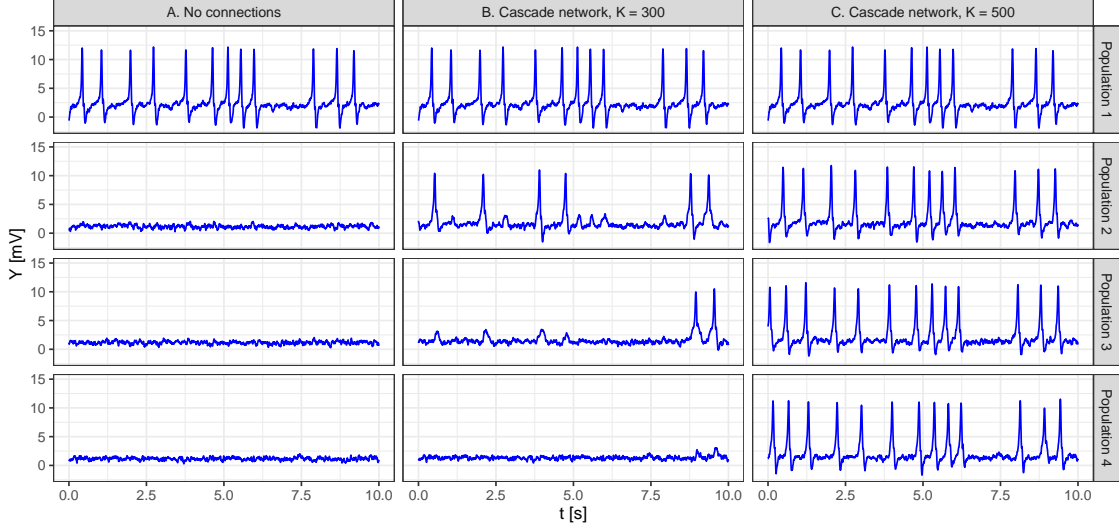


Figure 2: **Cascade network of four populations with one active population.** Simulated paths of  $Y$  in eq. (3) of  $N = 4$  neural populations. The standard values of Table 1,  $\mu = 90$  and  $\sigma = 500$  are used, except for Population 1 where  $A_1 = 3.6$  to make it active. Panel A:  $\rho_{jk} = 0$ ,  $j, k = 1, \dots, 4$ ,  $j \neq k$ . Panels B-C:  $\rho_{12}, \rho_{23}, \rho_{34} = 1$ . The coupling strength parameters  $K_{12}, K_{23}$  and  $K_{34}$  equal 300 (Panel B) and 500 (Panel C).

with gradients  $\nabla_P H_k(Q^k(t), P^k(t)) = P^k(t)$  and  $\nabla_Q H_k(Q^k(t), P^k(t)) = \Gamma_k^2 Q^k(t)$ , a *damping part* determined by the  $3 \times 3$ -dimensional diagonal matrix  $\Gamma_k = \text{diag}[a_k, a_k, b_k]$ , and a *non-linear displacement and coupling term*  $G_k : \mathbb{R}^{3N} \rightarrow \mathbb{R}^3$  given by

$$G_k(Q(t)) = \begin{pmatrix} A_k a_k \text{sig}(X_2^k(t) - X_3^k(t)) \\ A_k a_k \left( \mu_k + C_{2,k} \text{sig}(C_{1,k} X_1^k(t)) + \sum_{j=1, j \neq k}^N \rho_{jk} K_{jk} X_1^j(t) \right) \\ B_k b_k C_{4,k} \text{sig}(C_{3,k} X_1^k(t)) \end{pmatrix},$$

where  $Q = (Q^1, \dots, Q^N)^\top = (X_1^1, X_2^1, X_3^1, \dots, X_1^N, X_2^N, X_3^N)^\top$ . A compact Hamiltonian type formulation for the  $N$  coupled populations is then obtained by the process  $X := (Q, P)^\top$  with  $Q$  as above,  $3N$ -dimensional component  $P = (P^1, \dots, P^N)^\top = (X_4^1, X_5^1, X_6^1, \dots, X_4^N, X_5^N, X_6^N)^\top$  and  $3N$ -dimensional Wiener process  $W = (W^1, \dots, W^N)^\top = (W_4^1, W_5^1, W_6^1, \dots, W_4^N, W_5^N, W_6^N)^\top$ . In particular, the whole  $6N$ -dimensional stochastic Hamiltonian system is given by

$$d \begin{pmatrix} Q(t) \\ P(t) \end{pmatrix} = \begin{pmatrix} P(t) \\ -\Gamma^2 Q(t) - 2\Gamma P(t) + G(Q(t)) \end{pmatrix} dt + \begin{pmatrix} \mathbb{O}_{3N} \\ \Sigma \end{pmatrix} dW(t), \quad (5)$$

where  $\Gamma = \text{diag}[a_1, a_1, b_1, \dots, a_N, a_N, b_N]$  and  $\Sigma = \text{diag}[\epsilon_1, \sigma_1, \epsilon_1, \dots, \epsilon_N, \sigma_N, \epsilon_N]$  are  $3N \times 3N$ -dimensional diagonal matrices, and  $G : \mathbb{R}^{3N} \rightarrow \mathbb{R}^{3N}$  is given by  $G(Q) = (G_1(Q), \dots, G_N(Q))^\top$ .

**Remark 2.1** Including the coupling terms into the displacement function  $G : \mathbb{R}^{3N} \rightarrow \mathbb{R}^{3N}$  enables closed-form expressions of all required components of the splitting framework discussed in Section 3 for arbitrary  $N$ .

### 3 Simulation of the multi-population JR-NMM: Splitting integrators

Let  $0 = t_0 < \dots < t_m = T$  be a partition of the time interval  $[0, T]$  with equidistant time steps  $\Delta = t_{i+1} - t_i$  for  $i = 0, \dots, m-1$ ,  $m \in \mathbb{N}$ . As the solution  $X(t_i)$  of system (5) at the discrete time points  $t_i$  cannot be simulated exactly, we derive reliable approximations  $\tilde{X}(t_i)$  of  $X(t_i)$ , extending the numerical splitting method proposed in [1] for single neural populations to the multi-population case.

The splitting approach consists of the following three steps [6, 24]:

- (i) Split the equation for  $X(t)$  into  $d \in \mathbb{N}$  exactly solvable subequations for  $X^{[l]}(t)$ ,  $l = 1, \dots, d$ ;
- (ii) Derive the exact solutions (flows) of the  $d$  subequations over an increment of length  $\Delta$ , i.e., for initial value  $X^{[l]}(t_i)$ , the  $\Delta$ -flow is  $\varphi_{\Delta}^{[l]}(X^{[l]}(t_i)) = X^{[l]}(t_{i+1})$ ;
- (iii) Compose the  $d$  exact solutions in a suitable way. Prominent methods are the Lie-Trotter [40] and Strang [36] compositions, given by

$$\begin{aligned}\tilde{X}^{\text{LT}}(t_{i+1}) &= \left( \varphi_{\Delta}^{[1]} \circ \dots \circ \varphi_{\Delta}^{[d]} \right) \left( \tilde{X}^{\text{LT}}(t_i) \right), \\ \tilde{X}^{\text{S}}(t_{i+1}) &= \left( \varphi_{\Delta/2}^{[1]} \circ \dots \circ \varphi_{\Delta/2}^{[d-1]} \circ \varphi_{\Delta}^{[d]} \circ \varphi_{\Delta/2}^{[d-1]} \circ \dots \circ \varphi_{\Delta/2}^{[1]} \right) \left( \tilde{X}^{\text{S}}(t_i) \right),\end{aligned}$$

respectively. Note that the order of the compositions can be changed.

Despite having the same strong order of convergence, Strang compositions have been shown to outperform Lie-Trotter methods, yielding a better approximation of the true solution and preserving the model dynamics for larger time steps [1, 7, 9, 10, 17, 28, 41]. This is possibly due to the symmetry of the Strang splitting [1], its smaller mean biases [41] and its higher-order one-step predictions [28]. We therefore apply the Strang splitting for system (5), generalizing the Ornstein-Uhlenbeck integrator presented in [1]. Their Wiener integrator can be extended analogously.

**Step (i): Choice of subequations** We separate the non-linear term  $G(Q(t))$  of system (5), and consider the subequations

$$d \begin{pmatrix} Q^{[1]}(t) \\ P^{[1]}(t) \end{pmatrix} = \begin{pmatrix} P^{[1]}(t) \\ -\Gamma^2 Q^{[1]}(t) - 2\Gamma P^{[1]}(t) \end{pmatrix} dt + \begin{pmatrix} \mathbb{O}_{3N} \\ \Sigma \end{pmatrix} dW(t), \quad (6)$$

$$d \begin{pmatrix} Q^{[2]}(t) \\ P^{[2]}(t) \end{pmatrix} = \begin{pmatrix} 0_{3N} \\ G(Q^{[2]}(t)) \end{pmatrix} dt. \quad (7)$$

**Step (ii): Derivation of exact solutions** Write subequation (6) as

$$dX^{[1]}(t) = FX^{[1]}(t)dt + \Sigma_0 dW(t),$$

where

$$F = \begin{pmatrix} \mathbb{O}_{3N} & \mathbb{I}_{3N} \\ -\Gamma^2 & -2\Gamma \end{pmatrix}, \quad \Sigma_0 = \begin{pmatrix} \mathbb{O}_{3N} \\ \Sigma \end{pmatrix}.$$

Let  $X^{[1]}(t_i) = (Q^{[1]}(t_i), P^{[1]}(t_i))^{\top}$  denote the solution of system (6) at time  $t_i$ . The exact solution at time  $t_{i+1}$  is then given by

$$X^{[1]}(t_{i+1}) = \varphi_{\Delta}^{[1]} \left( X^{[1]}(t_i) \right) = e^{F\Delta} X^{[1]}(t_i) + \xi_i(\Delta),$$



where  $\xi_i(\Delta)$ ,  $i = 1, \dots, m$ , are independent  $6N$ -dimensional Gaussian random vectors with zero mean  $\mathbb{E}[\xi_i(\Delta)] = 0_{6N}$  and covariance matrix given by

$$\text{Cov}(\Delta) = \int_0^\Delta e^{F(\Delta-s)} \Sigma_0 \Sigma_0^\top \left( e^{F(\Delta-s)} \right)^\top ds.$$

For general matrices  $F$ , the exponential matrix  $e^{F\Delta}$  and the covariance matrix  $\text{Cov}(\Delta)$  may be costly to compute. However, due to the sparseness of  $F$  coming from the damped Hamiltonian term, both  $e^{F\Delta}$  and  $\text{Cov}(\Delta)$  can be expressed in closed-form for arbitrary  $N$  as

$$e^{F\Delta} = \begin{pmatrix} e^{-\Gamma\Delta} (\mathbb{I}_{3N} + \Gamma\Delta) & e^{-\Gamma\Delta} \Delta \\ -\Gamma^2 e^{-\Gamma\Delta} \Delta & e^{-\Gamma\Delta} (\mathbb{I}_{3N} - \Gamma\Delta) \end{pmatrix} =: \begin{pmatrix} \vartheta(\Delta) & \kappa(\Delta) \\ \vartheta'(\Delta) & \kappa'(\Delta) \end{pmatrix}$$

and

$$\text{Cov}(\Delta) = \begin{pmatrix} \frac{1}{4}\Gamma^{-3}\Sigma^2 (\mathbb{I}_{3N} + \kappa(\Delta)\vartheta'(\Delta) - \vartheta^2(\Delta)) & \frac{1}{2}\Sigma^2\kappa^2(\Delta) \\ \frac{1}{2}\Sigma^2\kappa^2(\Delta) & \frac{1}{4}\Gamma^{-1}\Sigma^2 (\mathbb{I}_{3N} + \kappa(\Delta)\vartheta'(\Delta) - \kappa'^2(\Delta)) \end{pmatrix}.$$

Denote the solution of the second subequation (7) at time  $t_i$  by  $X^{[2]}(t_i) = (Q^{[2]}(t_i), P^{[2]}(t_i))^\top$ . Since the first component of the right side of system (7) is zero and the second component only depends on  $Q$ , the exact solution at time  $t_{i+1}$  is given by

$$X^{[2]}(t_{i+1}) = \varphi_\Delta^{[2]} \left( X^{[2]}(t_i) \right) = X^{[2]}(t_i) + \Delta \begin{pmatrix} 0_{3N} \\ G(Q^{[2]}(t_i)) \end{pmatrix}.$$

**Step (iii): Composition of exact solutions** The Strang splitting integrator for (5) is then given by

$$\tilde{X}^S(t_{i+1}) = \left( \varphi_{\Delta/2}^{[2]} \circ \varphi_\Delta^{[1]} \circ \varphi_{\Delta/2}^{[2]} \right) \left( \tilde{X}^S(t_i) \right). \quad (8)$$

Using (8), a path of system (5) can be simulated by applying Algorithm 1. An analogous analysis as in [1] yields that the derived splitting scheme is mean-square convergent of order 1 and preserves the qualitative behaviour of the solution of (5), e.g., amplitudes of oscillations, marginal invariant densities and spectral densities.

---

**Algorithm 1** Strang splitting scheme for the  $N$ -population stochastic JR-NMM

**Input:** Initial value  $X_0$ , step size  $\Delta$ , number of time steps  $m$  in  $[0, T]$  and model parameters

**Output:** Approximated path of  $(X(t))_{t \in [0, T]}$  at discrete times  $t_i = i\Delta$ ,  $i = 0, \dots, m$ ,  $t_m = T$ .

---

- 1: Set  $\tilde{X}^S(t_0) = X_0$
  - 2: **for**  $i = 0 : (m - 1)$  **do**
  - 3: Set  $X^{[2]} = \tilde{X}^S(t_i) + \frac{\Delta}{2} \begin{pmatrix} 0_{3N} \\ G(\tilde{Q}^S(t_i)) \end{pmatrix}$
  - 4: Set  $X^{[1]} = e^{F\Delta} X^{[2]} + \xi_i(\Delta)$
  - 5: Set  $\tilde{X}^S(t_{i+1}) = X^{[1]} + \frac{\Delta}{2} \begin{pmatrix} 0_{3N} \\ G(Q^{[1]}) \end{pmatrix}$
  - 6: **end for**
  - 7: Return  $\tilde{X}^S(t_i)$ ,  $i = 0, \dots, m$ .
-

**Remark 3.1** *The Strang splitting integrator*

$$\tilde{X}^{S_2}(t_{i+1}) = \left( \varphi_{\Delta/2}^{[1]} \circ \varphi_{\Delta}^{[2]} \circ \varphi_{\Delta/2}^{[1]} \right) \left( \tilde{X}^{S_2}(t_i) \right)$$

is another possible choice. However, this composition requires to evaluate the more costly stochastic subsystem twice at every iteration step, generating twice as many pseudo-random numbers.

## 4 Adjusted SMC-ABC for network inference

In this section, we first revise the acceptance-rejection, reference-table acceptance-rejection and SMC-ABC schemes. Then, as the considered parameters of interest are both real and binary, we propose an adjusted SMC-ABC scheme, where the Gaussian proposal sampler within the “canonical” SMC-ABC algorithm is modified to account for both continuous (real-valued) model parameters and discrete ( $\{0, 1\}$ -valued) network parameters. Finally, we describe all underlying key ingredients (numerical scheme for data generation, summary statistics, proposal samplers, etc.). The resulting algorithm further develops the spectral density-based and measure-preserving ABC method proposed in [8] for ergodic SDEs with a univariate observed output process to multi-dimensional SDEs with coupled ergodic components, partially observed via  $N$  simultaneously recorded univariate time series. On the one hand, we replace the initially proposed reference table acceptance-rejection ABC with the more computationally efficient adjusted SMC-ABC (cf. Section 4.2). On the other hand, we generalise the summaries and distances to cope with the  $N > 1$  simultaneously observed coupled time series (cf. Section 4.3).

### 4.1 ABC schemes

Let  $\theta = (\theta_1, \dots, \theta_d)$  denote the parameter vector to be inferred from the observed data  $y$ . Denoting by  $\pi(\theta)$  the prior and by  $\mathcal{L}(y|\theta)$  the likelihood function, the posterior distribution  $\pi(\theta|y)$  satisfies

$$\pi(\theta|y) \propto \pi(\theta)\mathcal{L}(y|\theta).$$

In general, the likelihood function, and thus the true posterior, are not available for SDEs like (5). The idea of ABC is to replace the likelihood via a large amount of “synthetic” datasets simulated from the model, obtaining an approximate posterior  $\pi_{\text{ABC}}(\theta|y)$  targeting the true posterior  $\pi(\theta|y)$ .

Several ABC algorithms have been proposed throughout the years, see [34] for an overview. Among all, the simplest is *acceptance-rejection ABC* [4, 23, 34], consisting of three steps: (a) Sample  $\theta'$  from the prior  $\pi(\theta)$ ; (b) Conditioned on  $\theta'$ , simulate a synthetic dataset  $\tilde{y}_{\theta'}$  (here a path) from the observed output  $Y$ ; (c) Keep the sampled value  $\theta'$  if the distance  $D(\cdot, \cdot)$  between a vector of summary statistics  $s(\cdot)$  of the observed and simulated data is smaller than a threshold  $\delta > 0$ , i.e.,  $D(s(y), s(\tilde{y}_{\theta'})) < \delta$ . Steps (a)-(c) are then repeated until  $M$  draws are accepted, which typically happens after  $n \gg M$  drawings. This leads to the approximate acceptance-rejection ABC posterior

$$\pi(\theta|y) \approx \pi_{\text{ABC}}^{\delta}(\theta|s(y)) \propto \int \mathbb{1}_{\{D(s(y), s(\tilde{y}_{\theta'})) < \delta\}} \pi(\theta)\mathcal{L}(s(\tilde{y}_{\theta'})|\theta) ds.$$

Instead of keeping only the samples whose distance is smaller than some a priori fixed threshold  $\delta$ , the *reference table acceptance-rejection ABC scheme* [8, 12] first produces a *reference table*  $\{\theta_j, D_j\}$ ,  $j = 1 \dots, n$ , and then selects the threshold level  $\delta$  as the  $q$ -th percentile of the calculated distances  $D_j$ . This procedure has the computational advantage of fixing the number of drawings  $n$  in advance.

Acceptance-rejection ABC and its variant are computationally inefficient by construction, as the proposals  $\theta'$  are sampled from the prior distribution throughout. To tackle this, here we consider *SMC-ABC* [3, 13, 35], a sequential algorithm using proposal samplers constructed based on the kept sampled values (called *particles*) at the previous iteration  $r = 1, \dots, r_{\text{last}}$ , yielding

samplers defined on more likely parameter regions. This increases the acceptance probability of each particle, yielding intermediate approximate posterior distributions during several iterations which move closer and closer to the desired posterior. In particular, SMC-ABC works as follows: At iteration one, acceptance-rejection ABC is run, sampling from the prior distribution until  $M$  particles  $\Theta_1 = (\theta_1^{(1)}, \dots, \theta_1^{(M)})$  have been accepted, i.e., have yielded a distance smaller than an initial threshold  $\delta_1$ . Then, the initial weights are set to  $w_1 = (w_1^{(1)}, \dots, w_1^{(M)}) = (1/M, \dots, 1/M)$ . At iteration  $r > 1$ , a particle  $\theta$  is initially sampled from the set of kept candidates  $\Theta_{r-1}$  of the previous iteration with the corresponding weights  $w_{r-1}$  and then perturbed to a value  $\theta^* \sim \mathcal{K}(\cdot|\theta)$ , where  $\mathcal{K}$  is a suitable perturbation kernel. Such kernel is also known as proposal sampler or important sampler, and is commonly assumed to be Gaussian [13, 16], even if other possibilities have been proposed [27]. Here, we consider the optimized multivariate normal sampler as proposed in [16]. In particular, for given  $j, l \in \{1, \dots, M\}$  at iteration  $r$ , the perturbation kernel is given by

$$\mathcal{K}_r \left( \theta_r^{(j)} \middle| \theta_{r-1}^{(l)} \right) = (2\pi)^{-d/2} \left( \det \hat{\Sigma}_r \right)^{-1/2} \exp \left( -\frac{1}{2} \left[ \theta_r^{(j)} - \theta_{r-1}^{(l)} \right]^\top \hat{\Sigma}_r^{-1} \left[ \theta_r^{(j)} - \theta_{r-1}^{(l)} \right] \right), \quad (9)$$

where  $\hat{\Sigma}_r$  is twice the weighted empirical covariance matrix obtained from the previous population  $\Theta_{r-1}$  and  $\hat{\Sigma}_r^{-1}$  denotes its inverse. Synthetic data  $\tilde{y}_{\theta^*}$  are then simulated conditioned on the perturbed  $\theta^*$ , which is accepted if  $d(s(y), s(\tilde{y}_{\theta^*})) < \delta_r$ , with  $\delta_r < \delta_{r-1}$ . This is repeated until  $M$  particles  $\Theta_r = (\theta_r^{(1)}, \dots, \theta_r^{(M)})$  have been accepted, after which the corresponding important weights  $(\tilde{w}_r^{(1)}, \dots, \tilde{w}_r^{(M)})$  are computed as

$$\tilde{w}_r^{(j)} = \pi \left( \theta_r^{(j)} \right) / \sum_{l=1}^M w_{r-1}^{(l)} \mathcal{K}_r \left( \theta_r^{(j)} \middle| \theta_{r-1}^{(l)} \right)$$

and then normalised via

$$w_r^{(j)} = \tilde{w}_r^{(j)} / \sum_{l=1}^M \tilde{w}_r^{(l)}.$$

This procedure is then repeated over several iterations until a suitable stopping criterion is reached. The final SMC-ABC posterior is obtained by sampling from the particles kept at the last iteration  $r_{\text{last}}$  with probabilities given by the corresponding normalized weights.

## 4.2 Adjusted SMC-ABC algorithm for real and binary parameters

Here, we are interested in estimating both continuous (real-valued) model parameters and discrete ( $\{0, 1\}$ -valued) network parameters. To tackle this, we adapt the classical SMC-ABC algorithm with Gaussian proposal samplers to the specific case of additional  $\{0, 1\}$ -valued parameters, noting that the scheme can be adjusted to other distributions with finite support as well. The method is reported in Algorithm 2 and abbreviated as nSMC-ABC, where the ‘‘n’’ indicates that it includes network estimation.

We split the parameter vector  $\theta$  in continuous and discrete parts as

$$\theta := (\theta_c, \theta_d),$$

where  $\theta_c$  contains continuous (real-valued) model parameters, while  $\theta_d$  consists of the discrete ( $\{0, 1\}$ -valued) network parameters. We denote by  $c_n$  and  $d_n$  the dimensions of these two vectors, respectively, and their entries by  $\theta_c^k$ ,  $k = 1, \dots, c_n$ , and  $\theta_d^k$ ,  $k = 1, \dots, d_n$ . We write  $\Theta_{c,r}$  and  $\Theta_{d,r}$  to denote the  $M$  kept continuous (resp. discrete) particles at iteration  $r$ , where each particle  $\theta_r^{(j)}$  is represented as

$$\theta_r^{(j)} = (\theta_{c,r}^{(j)}, \theta_{d,r}^{(j)}), \quad j = 1, \dots, M.$$

We denote by  $\pi^c$  and  $\pi^d$  the prior distributions of  $\theta_c$  and  $\theta_d$ , and by  $\mathcal{K}_r^c$  and  $\mathcal{K}_r^d$  the perturbation kernels applied at the  $r$ -th iteration, respectively.

At iteration one, we run the canonical acceptance-rejection ABC, sampling from the prior (lines 2 – 10 of Algorithm 2). At iteration  $r > 1$ , we draw a particle  $\theta_{c,r}^{(j)}$  for the continuous parameters, which we sample from the weighted set  $\{\Theta_{c,r-1}, w_{r-1}\}$  (line 17 of Algorithm 2). However, differently from the classical SMC-ABC sampler, each entry of a particle  $\theta_{d,r}^{(j)}$  for the binary parameters is drawn from a Bernoulli distribution with probability given by the sample mean derived from the previous population (line 19 of Algorithm 2). Then, instead of jointly perturbing  $\theta_r^{(j)} = (\theta_{c,r}^{(j)}, \theta_{d,r}^{(j)})$  with a joint Gaussian proposal kernel  $\mathcal{K}_r$ , as done in the classical SMC-ABC, here we perturb them *independently* with respect to some continuous and discrete perturbation kernels  $\mathcal{K}_r^c$  and  $\mathcal{K}_r^d$  (lines 18 and 20 of Algorithm 2). This independence assumption comes from the fact that there is no natural relation between the network and continuous parameters, and it turns out to be beneficial, as it reduces the computational cost required to perturb a particle.

---

**Algorithm 2** Adjusted SMC-ABC for network inference (nSMC-ABC)

**Input:** Summaries  $s(y)$  of the observed data  $y$ , prior distributions  $\pi^c$  and  $\pi^d$ , perturbation kernels  $\mathcal{K}_r^c$  and  $\mathcal{K}_r^d$ , number of kept samples per iteration  $M$ , initial threshold  $\delta_1$

**Output:** Samples from the nSMC-ABC posterior

---

```

1: Set  $r = 1$ 
2: for  $j = 1 : M$  do
3:   repeat
4:     Sample  $\theta_d$  from  $\pi^d$  and  $\theta_c$  from  $\pi^c$ , and set  $\theta = (\theta_c, \theta_d)$ 
5:     Conditioned on  $\theta$ , simulate a synthetic dataset  $\tilde{y}_\theta$  from the observed output  $Y$ 
6:     Compute the summaries  $s(\tilde{y}_\theta)$ 
7:     Calculate the distance  $D = d(s(y), s(\tilde{y}_\theta))$ 
8:   until  $D < \delta_1$ 
9:   Set  $\theta_{d,1}^{(j)} = \theta_d$  and  $\theta_{c,1}^{(j)} = \theta_c$ 
10: end for
11: Initialize the weights by setting each entry of  $w_1 = (w_1^{(1)}, \dots, w_1^{(M)})$  to  $1/M$ 
12: repeat
13:   Set  $r = r + 1$ 
14:   Determine  $\delta_r < \delta_{r-1}$ 
15:   for  $j = 1 : M$  do
16:     repeat
17:       Sample  $\theta_c$  from the weighted set  $\{\Theta_{c,r-1}, w_{r-1}\}$ 
18:       Perturb  $\theta_c$  to obtain  $\theta_c^*$  from  $\mathcal{K}_r^c(\cdot|\theta_c)$ 
19:       Sample  $\theta_d^k$ ,  $k = 1, \dots, d_n$ , from Bernoulli( $\hat{p}_r^k$ ), where  $\hat{p}_r^k = \frac{1}{M} \sum_{l=1}^M \theta_{d,r-1}^{k,(l)}$ 
20:       Perturb  $\theta_d = (\theta_d^1, \dots, \theta_d^{d_n})$  to obtain  $\theta_d^*$  from  $\mathcal{K}_r^d(\cdot|\theta_d)$ 
21:       Conditioned on  $\theta^* = (\theta_c^*, \theta_d^*)$ , simulate a dataset  $\tilde{y}_{\theta^*}$  from the observed output  $Y$ 
22:       Compute the summaries  $s(\tilde{y}_{\theta^*})$ 
23:       Calculate the distance  $D = d(s(y), s(\tilde{y}_{\theta^*}))$ 
24:     until  $D < \delta_r$ 
25:     Set  $\theta_{d,r}^{(j)} = \theta_d^*$  and  $\theta_{c,r}^{(j)} = \theta_c^*$ 
26:     Set  $\tilde{w}_r^{(j)} = \pi^c(\theta_{c,r}^{(j)}) / \sum_{l=1}^M w_{r-1}^{(l)} \mathcal{K}_r^c(\theta_{c,r}^{(j)} | \theta_{c,r-1}^{(l)})$ 
27:   end for
28:   Normalise the weights  $w_r^{(j)} = \tilde{w}_r^{(j)} / \sum_{l=1}^M \tilde{w}_r^{(l)}$ , for  $j = 1, \dots, M$ 
29: until stopping criterion is reached
30: Return the final  $\Theta_{d,r_{\text{last}}}$  and  $\{\Theta_{c,r_{\text{last}}}, w_{r_{\text{last}}}\}$ .

```

---

**Remark 4.1** *The proposed nSMC-ABC Algorithm 2 is related to ABC for model selection as discussed in [39], in the sense that each possible network (obtained for a given combination of the*

binary parameters) may be interpreted as a model. Their algorithm samples real-valued parameter candidates conditioned on a given model and obtains the posterior distribution of the model based on the number of particles kept under each model. Thus, it is suitable for a low number of models, while in our case we would obtain a prohibitive number of possible models, namely  $2^{N(N-1)}$  (which equals, e.g., 4096 for  $N = 4$ ).

### 4.3 Ingredients of the nSMC-ABC algorithm

The accuracy and performance of any of the discussed ABC algorithms depend on various aspects, such as the numerical method used to simulate the data, the data summaries, the distances, the threshold values, the proposal kernels, etc. In the following, we describe the choice of these key ingredients.

**Choice of simulation method** We apply the Strang splitting integrator (8) described in Algorithm 1 to simulate datasets from the observed output process  $Y$  (3) of SDE (5).

**Choice of summary statistics** For the marginal behaviour of each population  $Y^k$ ,  $k = 1, \dots, N$ , we use the summary statistics proposed in [8]. In particular, taking advantage of the underlying geometric ergodicity, we map the  $N$ -dimensional time series  $y$  to the  $N$  estimated marginal invariant densities and spectral densities, the latter describing the dynamics in the frequency domain. Moreover, we include summaries capturing the interactions between populations, specifically the magnitude squared coherence (MSC), a statistic used to examine the similarity between two signals at various frequencies [38], and the cross-correlation as a function of lag.

Let  $R_k$  denote the auto-correlation function of  $Y^k$  and  $R_{jk}$  the cross-correlation function of  $Y_j$  and  $Y_k$ , that is

$$\begin{aligned} R_k(\tau) &= \mathbb{E}[Y^k(t)Y^k(t+\tau)], \quad k \in \{1, \dots, N\}, \\ R_{jk}(\tau) &= \mathbb{E}[Y^j(t)Y^k(t+\tau)], \quad j, k \in \{1, \dots, N\}, \quad j \neq k, \end{aligned}$$

where  $\tau$  denotes the time-lag. It holds that  $R_{jk}(\tau) = R_{kj}(-\tau)$ . The spectral density  $S_k$  of  $Y^k$  is given by the Fourier transform of  $R_k(\tau)$ , that is

$$S_k(\nu) = \mathcal{F}\{R_k\}(\nu) = \int_{-\infty}^{\infty} R_k(\tau)e^{-i2\pi\nu\tau} d\tau, \quad k \in \{1, \dots, N\},$$

where  $\nu$  denotes the frequency. Similarly, the cross-spectral density  $S_{jk}$  of  $Y^j$  and  $Y^k$  is given by

$$S_{jk}(\nu) = \mathcal{F}\{R_{jk}\}(\nu) = \int_{-\infty}^{\infty} R_{jk}(\tau)e^{-i2\pi\nu\tau} d\tau.$$

The MSC is defined as

$$Z_{jk}(\nu) := \frac{|S_{jk}(\nu)|^2}{S_j(\nu)S_k(\nu)}, \quad j, k \in \{1, \dots, N\}, \quad j \neq k,$$

where  $|\cdot|$  denotes the magnitude.

The summary functions are thus the marginal densities, denoted by  $f_k$ , the marginal spectral densities  $S_k$ ,  $k = 1, \dots, N$ , the symmetric MSCs  $Z_{jk}$ ,  $j, k = 1, \dots, N$ ,  $k > j$ , and the non-symmetric cross-correlations  $R_{jk}$ ,  $j, k = 1, \dots, N$ ,  $j \neq k$ . These functions are estimated from the available observations, see Section 4.4 for further details. Denoting the estimates by  $\hat{f}_k$ ,  $\hat{S}_k$ ,  $\hat{Z}_{jk}$  and  $\hat{R}_{jk}$ , respectively, the proposed summaries  $s(\cdot)$  of a dataset  $y$  are defined as

$$s(y) := \left\{ \hat{f}_k, \hat{S}_k, \hat{Z}_{jk}, \hat{R}_{jk} \right\}. \quad (10)$$

**Choice of distance measure** Following [8], as distances between the summary functions (10) of the observed and simulated datasets, we use the integrated absolute error (IAE) given by

$$\text{IAE}(g_1, g_2) := \int_{\mathbb{R}} |g_1(x) - g_2(x)| dx \in \mathbb{R}^+,$$

approximated by rectangular integration. The distance between the summaries of the observed dataset  $y$  and a simulated dataset  $\tilde{y}_\theta$  is then defined as

$$\begin{aligned} D(s(y), s(\tilde{y}_\theta)) &:= v_1 \frac{1}{N} \sum_{k=1}^N \text{IAE}(\hat{S}_k, \tilde{S}_k) + v_2 \frac{1}{N(N-1)/2} \sum_{j=1, k>j}^N \text{IAE}(\hat{Z}_{jk}, \tilde{Z}_{jk}) \\ &+ v_3 \frac{1}{N(N-1)} \sum_{j,k=1, j \neq k}^N \text{IAE}(\hat{R}_{jk}, \tilde{R}_{jk}) + v_4 \frac{1}{N} \sum_{k=1}^N \text{IAE}(\hat{f}_k, \tilde{f}_k), \end{aligned} \quad (11)$$

where  $\{\hat{f}_k, \hat{S}_k, \hat{Z}_{jk}, \hat{R}_{jk}\}$  and  $\{\tilde{f}_k, \tilde{S}_k, \tilde{Z}_{jk}, \tilde{R}_{jk}\}$  denote the summaries of the observed and simulated datasets, respectively. The values  $v_l \geq 0$ ,  $l = 1, 2, 3, 4$ , are weights guaranteeing that the different summary functions have a comparable impact on the distance measure (cf. Section 4.4).

**Choice of prior distributions** We use independent uniform priors

$$\theta_c^k \sim \text{U}(\theta_{c,\min}^k, \theta_{c,\max}^k), \quad k = 1, \dots, c_n,$$

for the continuous parameters and independent Bernoulli priors

$$\theta_d^k \sim \text{Bernoulli}(p), \quad p = \frac{1}{2}, \quad k = 1, \dots, d_n,$$

for the discrete parameters. In particular,

$$\begin{aligned} \pi^c(\theta_c) &= \prod_{k=1}^{c_n} \pi(\theta_c^k) = \prod_{k=1}^{c_n} \frac{1}{\theta_{c,\max}^k - \theta_{c,\min}^k}, \\ \pi^d(\theta_d) &= \prod_{k=1}^{d_n} \pi(\theta_d^k) = \prod_{k=1}^{d_n} \left(\frac{1}{2}\right)^{\theta_d^k} \left(\frac{1}{2}\right)^{1-\theta_d^k} = \frac{1}{2^{d_n}}. \end{aligned}$$

**Choice of proposal samplers** For the continuous parameters, we choose  $\mathcal{K}_r^c$  as in (9), i.e., the optimized Gaussian sampler [16]. A particle  $\theta_c$  sampled at iteration  $r$  according to the normalized weights of  $w_{r-1}$  (line 17 of Algorithm 2) is thus perturbed to  $\theta_c^*$ , a realization of the multivariate normal distribution  $\mathcal{N}(\theta_c, \hat{\Sigma}_{c,r})$ , where  $\hat{\Sigma}_{c,r}$  is twice the weighted covariance matrix obtained from the previous population  $\Theta_{c,r-1}$  (line 18 of Algorithm 2).

For the discrete parameters, a value  $\theta_d^k$ ,  $k = 1, \dots, d_n$ , sampled from a Bernoulli distribution at iteration  $r$  (line 19 of Algorithm 2) is either kept (with probability  $q_{\text{stay}}$ ) or perturbed to  $1 - \theta_d^k$  (line 20 of Algorithm 2). An explicit expression of the respective kernel  $\mathcal{K}_r^d$  is given by

$$\mathcal{K}_r^d \left( \theta_{d,r}^{(j)} \middle| \theta_{d,r-1}^{(l)} \right) = \prod_{k=1}^{d_n} \mathcal{K}_r^{d,k} \left( \theta_{d,r}^{k,(j)} \middle| \theta_{d,r-1}^{k,(l)} \right) = \prod_{k=1}^{d_n} \left( p_r^{k,(l)} \right)^{\theta_{d,r}^{k,(j)}} \left( 1 - p_r^{k,(l)} \right)^{1 - \theta_{d,r}^{k,(j)}}, \quad (12)$$

where

$$p_r^{k,(l)} = \begin{cases} q_{\text{stay}}, & \text{if } \theta_{d,r-1}^{k,(l)} = 1 \\ 1 - q_{\text{stay}}, & \text{if } \theta_{d,r-1}^{k,(l)} = 0 \end{cases}.$$

Throughout this work, the probability  $q_{\text{stay}}$  is fixed across iterations (cf. Section 4.4). Alternatively, such probability could also vary, e.g., it may depend on some statistics of the previous population or the number of iterations.

**Choice of threshold levels** The initial threshold  $\delta_1$  is obtained by a reference table acceptance-rejection ABC pilot run. Under the given prior, we produce  $10^4$  distances and then choose  $\delta_1$  as their median. For  $r > 1$ , the threshold  $\delta_r$  is chosen as the median of the  $M$  distances computed at the previous iteration if the acceptance rate of particles at the previous iteration is larger than 1%. Otherwise  $\delta_r$  is chosen as the 75th percentile of the  $M$  distances computed at iteration  $r - 1$ .

**Choice of stopping criterion** The algorithm is stopped after the acceptance rate of particles at a certain iteration has dropped below a prefixed threshold (cf. Section 4.4).

## 4.4 Implementation details

The nSMC-ABC method is coded using the statistical software R [30], combined with the package Rcpp [15]. Algorithm 1 is coded in C++ and then integrated into the R-Code for Algorithm 2. The for-loops of Algorithm 2 are parallelized using the packages `doParallel` and `foreach`. All experiments are run on a multiple core High-Performance-Cluster at the University of Klagenfurt.

The summaries (10) are computed as follows: Estimates of the spectral densities and MSCs are obtained using smoothed periodogram estimators. We apply the R-function `crossSpectrum` from the package `IRISSeismic` to obtain the spectral densities  $\hat{S}_k$  and the MSCs  $\hat{Z}_{jk}$ . Estimates of the densities  $\hat{f}_k$  and cross-correlation functions  $\hat{R}_{jk}$  are obtained using the (Gaussian) kernel density estimator `density` and the R-function `ccf` from the `stats`-package, respectively. The weights  $v_l$ ,  $l = 1, 2, 3, 4$ , in the distance function (11) are obtained as follows: We set  $v_1 = 1$  and obtain  $v_2, v_3, v_4$  by dividing the average area below the spectral densities of the observed data by the average area below the MSCs, cross-correlation functions and densities of the observed data, respectively (the latter equals 1).

The multivariate normal proposal sampler (9) is calculated using the R-package `mvnfast`, which provides computationally efficient tools (e.g., through C++ code) for the multivariate normal distribution. In particular,  $\theta_c^* \sim \mathcal{N}(\theta_c, \hat{\Sigma}_{c,r})$  is sampled using the R-function `rmvn`, and the multivariate normal density is computed with the R-function `dmvn` (lines 18 and 26 of Algorithm 2). The weighted covariance matrix  $\hat{\Sigma}_{c,r}$  is estimated with the R-function `cov.wt` from the `stats`-package. The probability  $q_{\text{stay}}$  of the discrete perturbation kernel (12) is set to 0.9 throughout. The number  $M$  of kept particles per iteration and the threshold for the stopping criterion are set to 500 and 0.1%, respectively, in all experiments.

Finally, sample code is provided at <https://github.com/IreneTubikanec/networkABC>

## 5 Network inference from simulated data

In this section, we test the performance of the proposed nSMC-ABC algorithm on simulated datasets. All reference datasets are generated up to time  $T = 20$  with time step  $10^{-4}$ , and then subsampled with observation time step  $\Delta = 2 \cdot 10^{-3}$ , yielding  $10^4$  discrete time observations of an  $N$ -dimensional process.

### 5.1 Parameter vector and prior distribution

To reduce the number of continuous parameters in the model, we assume that the coupling strength between two populations decreases with increasing distance, where the distance is defined by the difference between their subindices. In particular, for  $j, k \in \{1, \dots, N\}$  with  $j \neq k$ , define

$$K_{jk} := c^{|j-k|-1} L,$$

where  $L > 0$  is a coupling strength parameter and the parameter  $0 \ll c < 1$  describes how fast the network coupling strength decreases with increasing distance between populations. As the model parameters  $A_k$ ,  $k \in \{1, \dots, N\}$ , also play a central role in the (non-)activation of neural populations (see Section 2), we also aim to infer them. The parameters  $\mu_k$  and  $\sigma_k$  are fixed to 90 and 500, respectively, and the remaining continuous parameters are fixed according to the

standard values reported in Table 1. Hence, applying the nSMC-ABC Algorithm 2, the goal is to infer the  $(N + 2 + N(N - 1))$ -dimensional parameter vector

$$\theta = (\underbrace{A_1, \dots, A_N, L, c}_{\theta_c}, \underbrace{\text{vec}(\mathcal{P})}_{\theta_d}),$$

where the discrete parameters  $\theta_d = \text{vec}(\mathcal{P})$  are given by

$$\mathcal{P} = \begin{pmatrix} - & \rho_{12} & \dots & \dots & \rho_{1N} \\ \rho_{21} & - & \ddots & & \vdots \\ \vdots & \ddots & \ddots & \ddots & \vdots \\ \vdots & & \ddots & - & \rho_{N-1N} \\ \rho_{N1} & \dots & \dots & \rho_{NN-1} & - \end{pmatrix},$$

with  $\rho_{jk} \in \{0, 1\}$ ,  $j, k = 1, \dots, N$ ,  $j \neq k$ .

The prior distributions for  $\theta_c$  are independent continuous uniforms with supports,

$$A_k \sim \text{U}(2, 4), \quad k = 1, \dots, N, \quad L \sim \text{U}(100, 2000), \quad c \sim \text{U}(0.5, 1).$$

The prior distributions for  $\theta_d$  are independent Bernoulli distributions with equal probabilities,

$$\rho_{jk} \sim \text{Bernoulli}(p), \quad p = \frac{1}{2}, \quad j, k \in \{1, \dots, N\}, \quad j \neq k. \quad (13)$$

## 5.2 Estimation results

We focus on  $N = 4$  neural populations and consider three scenarios, i.e., a cascade structure (used to simulate the data in Figure 2), a partially and a fully connected network. The three settings are visualised in Figure 3. We apply Algorithm 2 to reference datasets (4 simultaneously observed univariate time series, each with  $10^4$  data points) generated under these scenarios to estimate  $\theta$ .

**Setting 1: Cascade structure** The reference data  $y$  of the cascade scenario is simulated under

$$\theta = (A_1, A_2, A_3, A_4, L, \text{vec}(\mathcal{P})) = (3.6, 3.25, 3.25, 3.25, 700, \text{vec}(\mathcal{P})), \quad (14)$$

with  $\rho_{12} = \rho_{23} = \rho_{34} = 1$  and all other  $\rho_{jk} = 0$ . The network is visualised in Figure 3a. It shows a similar behaviour as the data in the right column of Figure 2. In this scenario, the parameter  $c$  is not present and is excluded from  $\theta$ .

Figure 4a shows the marginal posterior densities (blue lines) and the uniform prior densities (horizontal red lines) of the continuous parameters. The true parameter values used to generate the data are indicated by vertical solid green lines, and the dotted black lines are the weighted posterior means. They are given by

$$(\hat{A}_1, \hat{A}_2, \hat{A}_3, \hat{A}_4, \hat{L}) = (3.615, 3.248, 3.252, 3.254, 705.6),$$

closely resembling the true values in (14). In Figure 4b, we report the marginal posterior histograms of the discrete parameters, representing the coupling directions. The true values (vertical dashed green lines) coincide with the nSMC-ABC posterior modes. To summarize, Algorithm 2 yields unimodal and narrow marginal posterior densities of all relevant continuous model parameters, covering the true values. Moreover, the obtained nSMC-ABC marginal posteriors for the binary parameters are Bernoulli distributed with probabilities equal to the true parameters  $\rho_{jk}$ , successfully recovering the entire network structure.



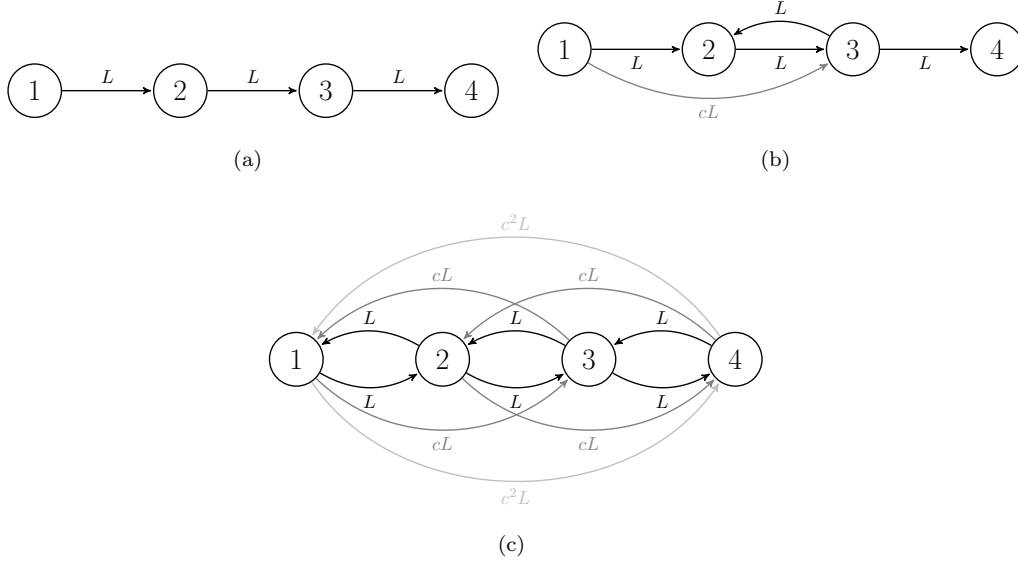


Figure 3: **Network structures** of  $N = 4$  neural populations used in the simulations. (a) Cascade network structure with equal coupling strengths. (b) Partially connected network. (c) Fully connected network.

**Setting 2: Partially connected network** The reference data  $y$  of the partially connected scenario (visualised in Figure 3b) is generated using

$$\theta = (A_1, A_2, A_3, A_4, L, c, \text{vec}(\mathcal{P})) = (3.6, 3.25, 3.25, 3.25, 700, 0.8, \text{vec}(\mathcal{P})),$$

with  $\rho_{12} = \rho_{23} = \rho_{34} = \rho_{13} = \rho_{32} = 1$  and all other  $\rho_{jk} = 0$ . The parameter  $c$  is included since there is a connection from Population 1 to Population 3.

Figure 5a shows the marginal posterior densities (blue lines) and the uniform prior densities (horizontal red lines) of the continuous parameters  $\theta_c^k, k = 1, \dots, 6$ . The true parameter values are shown by the vertical solid green lines, and the dotted black lines are the weighted nSMC-ABC posterior means, given by

$$(\hat{A}_1, \hat{A}_2, \hat{A}_3, \hat{A}_4, \hat{L}, \hat{c}) = (3.614, 3.222, 3.259, 3.203, 693.4, 0.726).$$

As before, we obtain unimodal marginal posterior densities covering the true values for  $L$  and  $A_k, k = 1, \dots, 4$ . However, the inference for  $c$  is not satisfactory. This is probably due to the low information about  $c$  available in the data, as it only enters through the connection from Population 1 to Population 3.

Figure 5b shows the nSMC-ABC marginal distributions of the discrete parameters  $\theta_d^k, k = 1, \dots, 12$ . As before, the posterior modes coincide with the true values of the  $\rho_{jk}$  (vertical dashed green lines). Thus, the network structure is correctly identified.

**Setting 3: Fully connected network** In the fully connected scenario (Figure 3c) the reference data  $y$  is obtained under

$$\theta = (A_1, A_2, A_3, A_4, L, c, \text{vec}(\mathcal{P})) = (3.25, 3.25, 3.25, 3.25, 700, 0.8, \text{vec}(\mathcal{P})),$$

with  $\rho_{jk} = 1$  for all  $j, k$ .

Figure 6a depicts the marginal posterior densities (blue lines) and the uniform prior densities (horizontal red lines) of the continuous parameters, the true parameter values (vertical green lines), and the weighted nSMC-ABC posterior means (dotted black lines), given by

$$(\hat{A}_1, \hat{A}_2, \hat{A}_3, \hat{A}_4, \hat{L}, \hat{c}) = (3.235, 3.247, 3.228, 3.246, 719.7, 0.791).$$

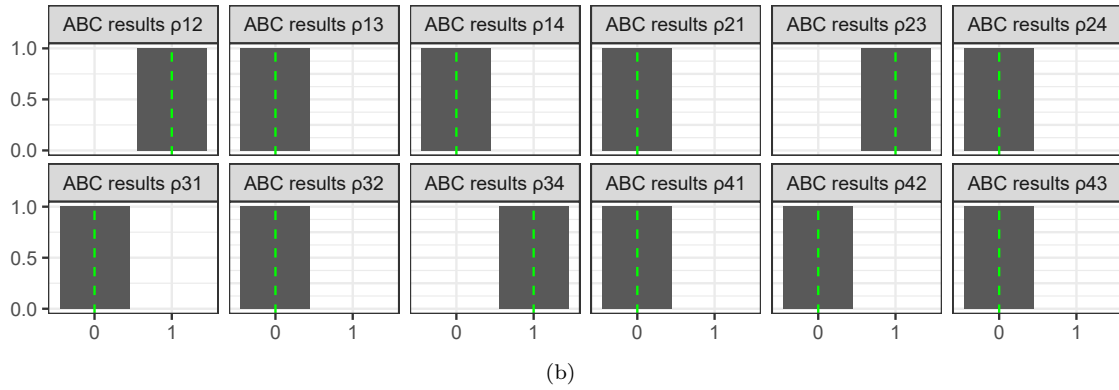
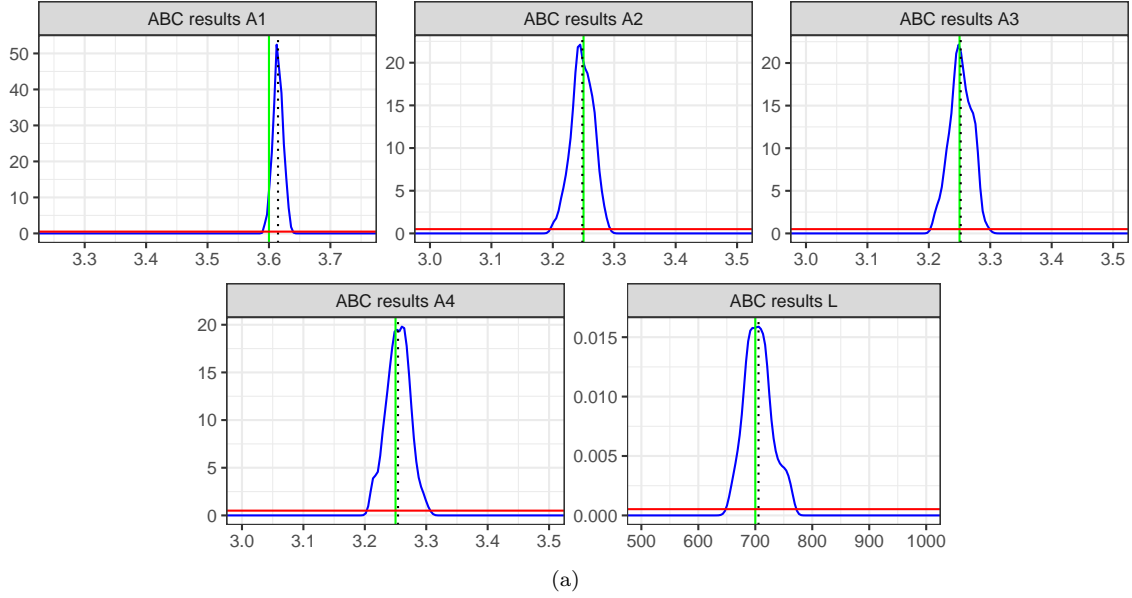
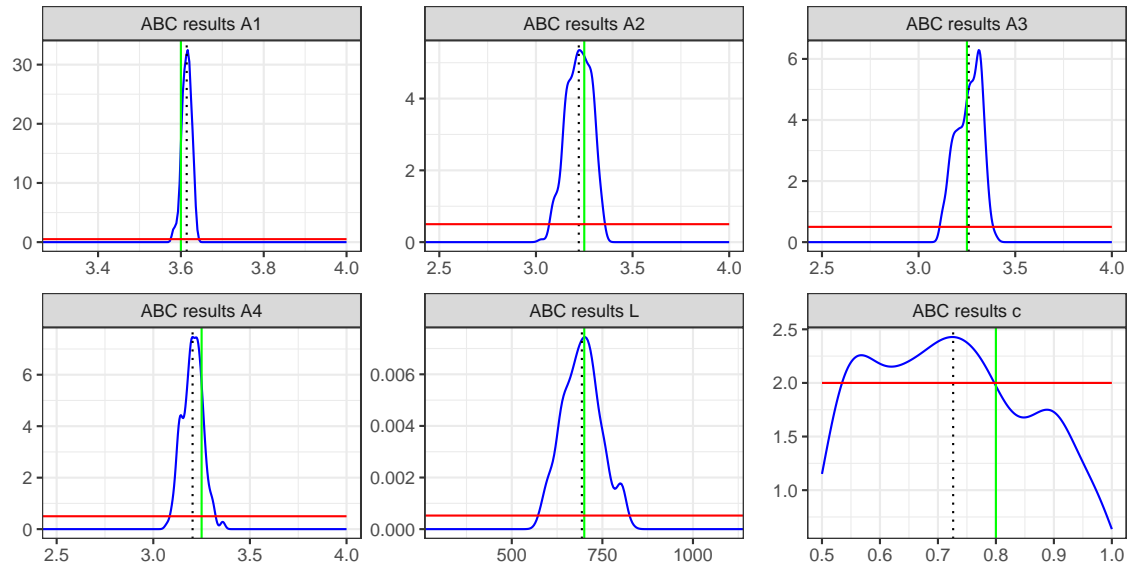
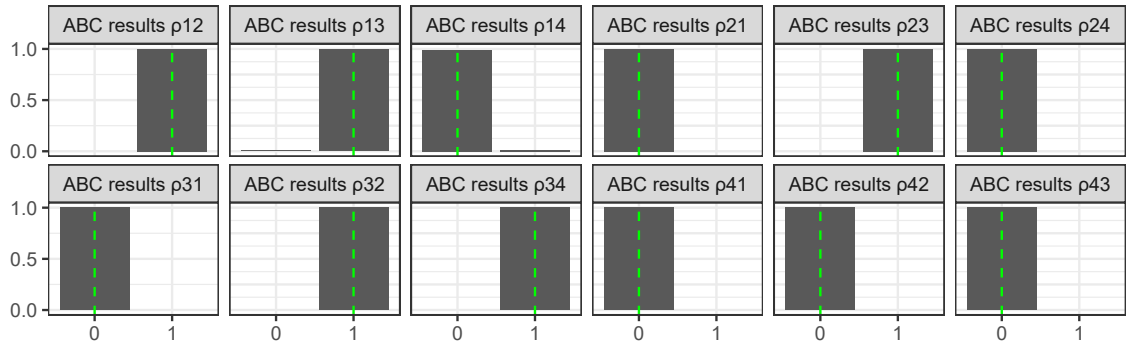


Figure 4: **Cascade network.** (a) nSMC-ABC marginal posterior densities (blue lines) compared to the prior densities (horizontal red lines) of the continuous parameters in the cascade scenario, see Figure 3a. The vertical green lines and the dotted black lines are the true parameter values and the weighted posterior means, respectively. (b) nSMC-ABC marginal posterior distributions of the network coupling parameters in the cascade scenario. The vertical dashed green lines are the true parameter values.

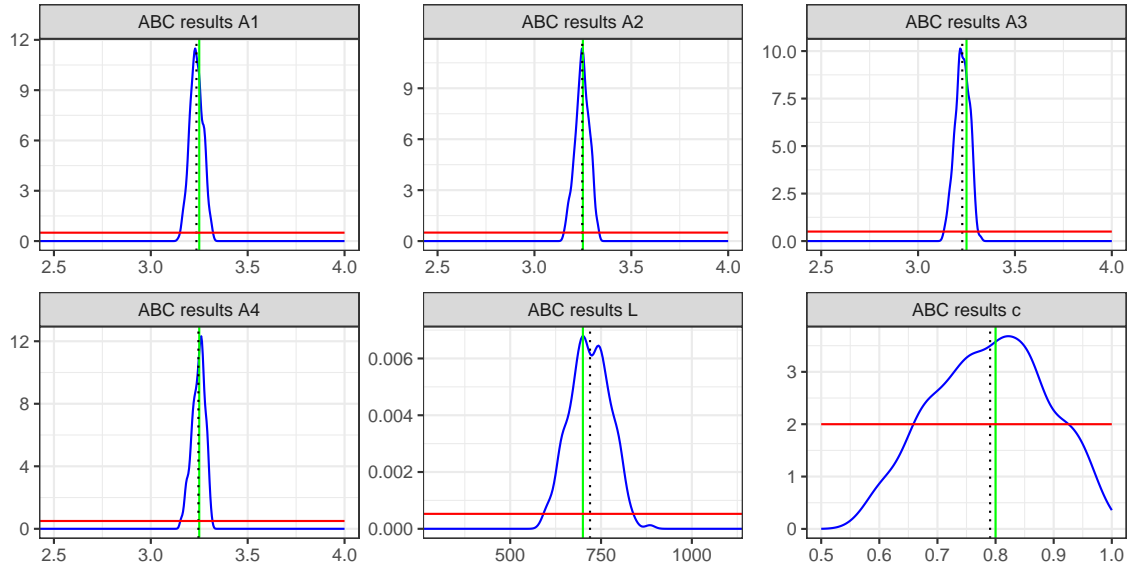


(a)

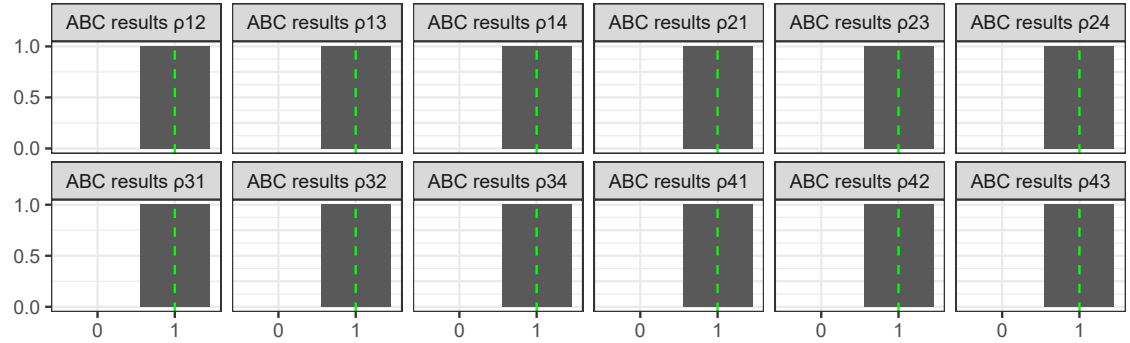


(b)

Figure 5: **Partially connected network.** (a) nSMC-ABC marginal posterior densities (blue lines) compared to the prior densities (horizontal red lines) of the continuous parameters in the partially connected scenario, see Figure 3b. The vertical green lines and the dotted black lines are the true parameter values and the weighted posterior means, respectively. (b) nSMC-ABC marginal posterior distributions of the network coupling parameters in the partially connected scenario. The vertical dashed green lines are the true parameter values.



(a)



(b)

Figure 6: **Fully connected network.** (a) nSMC-ABC marginal posterior densities (blue lines) compared to the prior densities (horizontal red lines) of the continuous parameters in the fully connected scenario, see Figure 3c. The vertical green lines and the dotted black lines are the true parameter values and the weighted posterior means, respectively. (b) nSMC-ABC marginal posterior distributions of the network coupling parameters in the fully connected scenario. The vertical dashed green lines are the true parameter values.

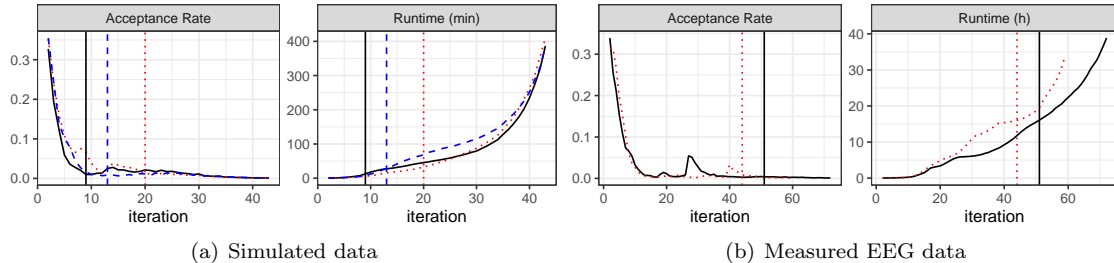


Figure 7: **Acceptance rate and runtime** as functions of the iterations  $r$  of Algorithm 2. (a) Simulated data, time measured in minutes. The vertical lines mark those iterations from which the correct network is inferred, i.e., the coupling parameters  $\rho_{jk}$  are correctly estimated via the posterior modes. The solid black, dotted red and dashed blue lines correspond to the cascade, partially connected and fully connected scenario, respectively. (b) EEG data with  $N = 4$  channels, time measured in hours. The dotted red and solid black lines correspond to the before and during seizure periods, respectively. The vertical lines mark that iteration from which the network estimate does not change anymore.

As in the previous two scenarios, we obtain unimodal and narrow marginal nSMC-ABC posterior densities, covering the true values, for  $L$  and  $A_k$ ,  $k = 1, \dots, 4$ . Compared to the partially connected case, we obtain slightly better inference for  $c$ . Similar to the cascade and partially connected scenarios, the network structure is correctly identified, see Figure 6b.

**Acceptance rate, runtime and effective sample size** In Figure 7a, we report the acceptance rate of particles and the runtime (in min) of Algorithm 2 as functions of the iterations  $r$ , for the cascade (solid black lines), partially connected (dotted red lines) and fully connected (dashed blue lines) network scenarios. In all settings, Algorithm 2 terminates after iteration 43, where the acceptance rate drops below the threshold of 0.1%. The slope of both the acceptance rate and the runtime curve is comparable in the three scenarios. Remarkably, the correct network is inferred (i.e., the marginal posterior modes of the discrete parameters coincide with the true values) earlier than the algorithm terminates, i.e., from iteration 9, 20 and 13 for the cascade, partially connected and fully connected scenarios, respectively. These iteration numbers are indicated by the vertical lines. Note, however, that while the marginal posterior modes at these iterations are the same as at the final one, the marginal posterior distributions itself may still differ.

Finally, we have also considered the “effective sample size” (ESS),  $1 \leq \text{ESS} \leq M$ , calculated at iteration  $r$  as  $1/(\sum_{l=1}^M (w_r^{(l)})^2)$ , as a measure of the effectiveness of the SMC sampler, that is, intuitively, how many of the  $M$  particles are “relevant”. The ESS of the three scenarios look similar, mainly oscillating between 350 and 450 (recall that  $M$  is set to 500 here), with overall median across the iterations equal to 411, 418 and 407, respectively (figure not reported).

## 6 Network inference from EEG data with epileptic activity

After validating the proposed algorithm on simulated data, we now use it to estimate the connectivity structure from real EEG data.

### 6.1 Description of the data

In [33], a study on 22 patients from the Children’s Hospital Boston, who experience epileptic seizures, was presented. The aim of the study was to detect seizure periods in multiple hour EEG recordings of each individual. The data are available at <https://www.physionet.org/content/chbmit/1.0.0/>.

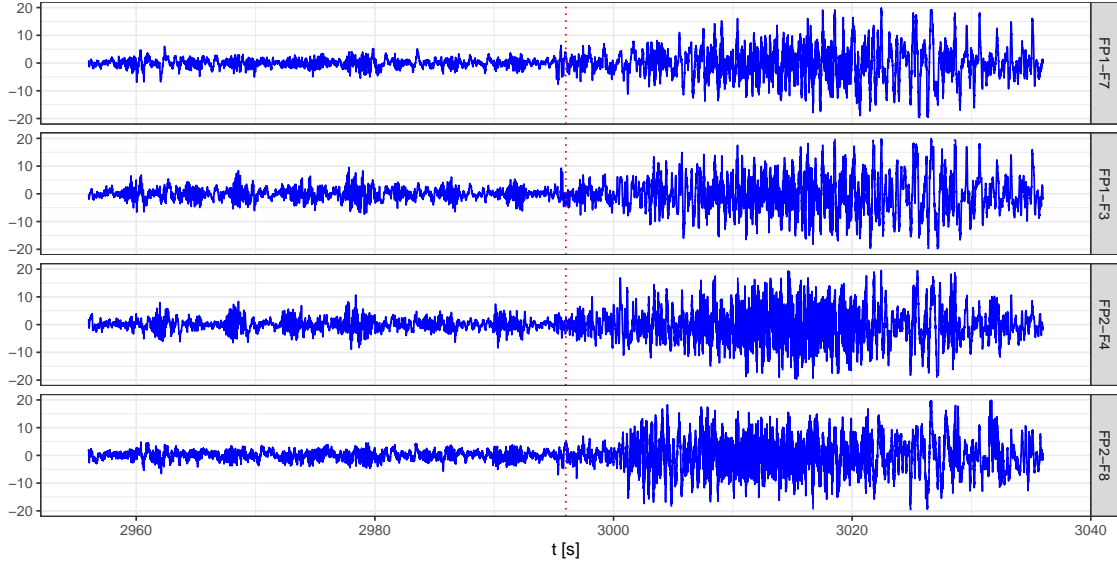


Figure 8: **EEG recordings of a 11 year old female patient.** The interval  $[2996, 3036]s$  (measurements to the right of the vertical dotted red lines) has been defined as a seizure in [33].

Here, we analyse recordings of an 11 year old female patient prior to and during seizure, from the edf-file `chb01_03` in the above link. Following [26, 32], we consider the four channels FP1-F7, FP1-F3, FP2-F4 and FP2-F8, where FP refers to the frontal lobes (the first two on the left hemisphere and the second two on the right) and F to a set of electrodes placed behind them. The electrode locations are according to the international 10–20 system for EEG measurements. The recordings are visualised in Figure 8, where the vertical dotted red lines separate the data into the period before and during seizure, lasting 40 seconds [s] each, with the period from 2996 to 3036s classified as a seizure in [33]. The data are sampled with a frequency of 256 Hz, corresponding to 10240 discrete time measurements during each of the two 40s periods. To put the recordings on the same scale as the model, we rescale the data by multiplying each data point with the factor 0.05.

## 6.2 Inference

We now fit the stochastic multi-population JR-NMM to the data prior to and during seizure, aiming to infer the underlying network structure as well as relevant continuous model parameters in these two regimes via our proposed nSMC-ABC Algorithm 2.

**Parameter vector and prior distribution** In the following, we identify the channels FP1-F7, FP1-F3, FP2-F4 and FP2-F8 by Population 1, 2, 3, and 4, respectively. As the distance between channels on different hemispheres is larger than that on the same, we have that the distance between the channels FP1-F3 and FP2-F4 is larger than that between FP1-F7 and FP1-F3 or between FP2-F4 and FP2-F8. For this reason, we assume the following matrix of coupling strength parameters

$$K = \begin{pmatrix} - & K_{12} & K_{13} & K_{14} \\ K_{21} & - & K_{23} & K_{24} \\ K_{31} & K_{32} & - & K_{34} \\ K_{41} & K_{42} & K_{43} & - \end{pmatrix} = \begin{pmatrix} - & L & c^2L & c^3L \\ L & - & cL & c^2L \\ c^2L & cL & - & L \\ c^3L & c^2L & L & - \end{pmatrix},$$

with unknown  $L$  and  $c$ . Moreover, we assume the activation parameters  $A_k$ ,  $k = 1, \dots, 4$ , the noise intensity parameters  $\sigma_l := \sigma_1 = \sigma_2$  (left hemisphere) and  $\sigma_r := \sigma_3 = \sigma_4$  (right hemisphere) as well

as the input parameters  $\mu_l := \mu_1 = \mu_2$  (left hemisphere) and  $\mu_r := \mu_3 = \mu_4$  (right hemisphere) to be unknown. For the remaining parameters, we use the standard values reported in Table 1, except for setting  $b = 20$  and  $C = 70$  (values chosen based on pilot experiments). We thus aim to infer the  $(10 + 12)$ -dimensional parameter vector

$$\theta = (A_1, A_2, A_3, A_4, L, c, \sigma_l, \sigma_r, \mu_l, \mu_r, \text{vec}(\mathcal{P})).$$

We choose independent continuous uniform prior distributions for  $\theta_c$  with broad supports,

$$A_k \sim \text{U}(1, 30), \quad k = 1, \dots, 4, \quad L \sim \text{U}(100, 5000), \quad c \sim \text{U}(0.5, 1), \\ \sigma_l, \sigma_r \sim \text{U}(100, 15000), \quad \mu_l, \mu_r \sim \text{U}(1, 300).$$

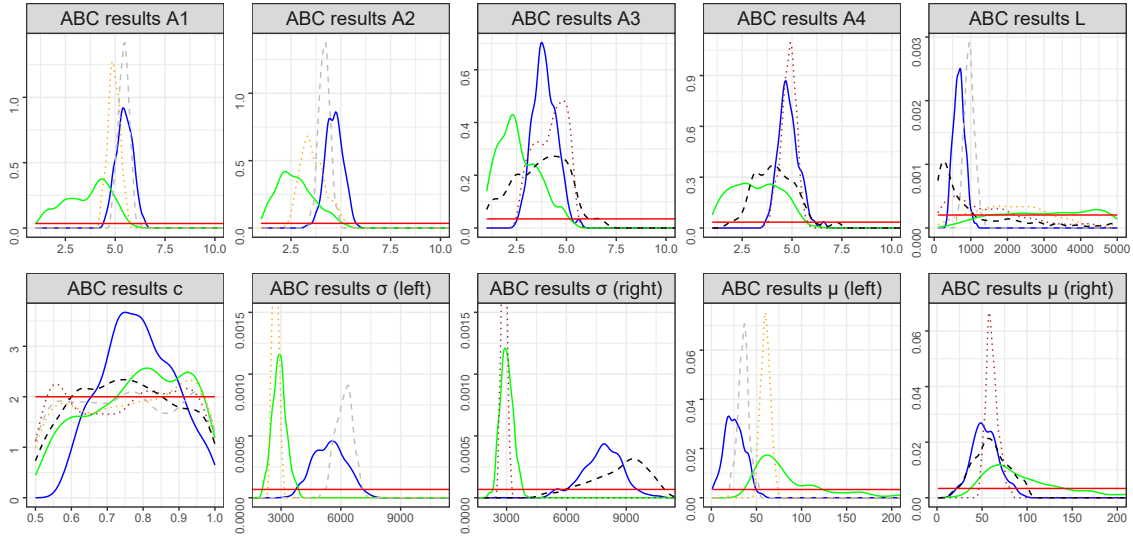
The priors for  $\theta_d$  are independent Bernoulli distributions with equal probabilities, see (13).

**Estimation results** In Figure 9a, we report the marginal posterior densities (green lines: before seizure, blue lines: during seizure) and the uniform prior densities (horizontal red lines) of the continuous parameters  $\theta_c^k, k = 1, \dots, 10$ . All posteriors for the parameters during seizure are unimodal, showing a clear update of the priors. Comparing the individual population parameters  $A_k, k = 1, \dots, 4$ , for the two periods, there is a larger activation in all 4 neural populations during seizure. Moreover, as expected, the posteriors of the noise intensity parameters  $\sigma_l$  and  $\sigma_r$  assume larger values in both brain hemispheres during seizure. While we obtain a clear estimate of the posterior for the coupling strength parameter  $L$  during seizure, this is not the case before seizure. However, the posterior suggests a coupling strength far away from zero also in this scenario.

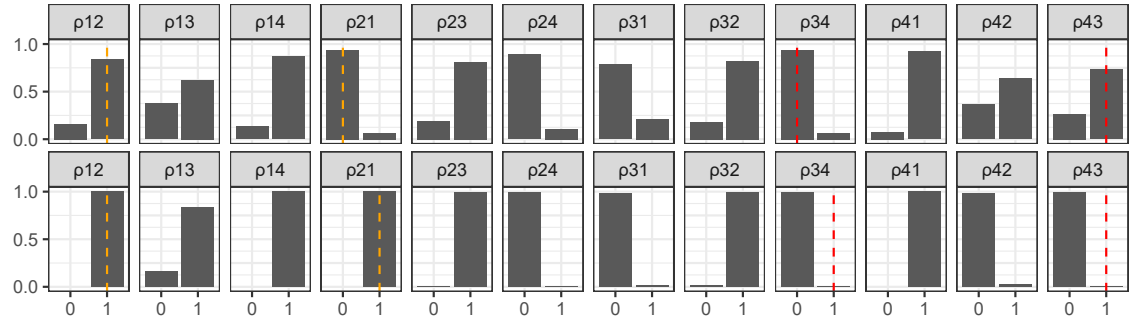
Figure 9b shows the marginal posterior histograms for the coupling direction parameters  $\theta_d^k, k = 1, \dots, 12$  (top panels: before seizure, bottom panels: during seizure). The posteriors during the seizure period provide a clear connectivity structure, with the inferred network visualised in Figure 10b. The inferred network prior to seizure (Figure 10a) is similar, except for a missing connection from Population 2 (FP1-F3) to Population 1 (FP1-F7) on the left hemisphere, present during seizure. The inferred network also differs for  $\rho_{42}$  and  $\rho_{43}$ , with a connection from Population 4 (FP2-F8) to 2 (FP1-F3) and to 3 (FP2-F4) present only before seizure. However, for these parameters the results are less evident (estimated probabilities for a connection smaller than 0.75 in the before seizure scenario).

To further investigate the differences, if any, between the two hemispheres, we also apply our nSMC-ABC Algorithm 2 only to the two channels from the same hemisphere, i.e., left hemisphere (FP1-F7 and FP1-F3) and right hemisphere (FP2-F8 and FP2-F4), both before and during seizure. The dotted orange/dashed grey (left hemisphere) and dotted brown/dashed black (right hemisphere) lines in Figure 9a are the marginal nSMC-ABC posteriors of the corresponding parameters before/during seizure. The dashed orange (left hemisphere) and red (right hemisphere) vertical lines in Figure 9b indicate the inferred connections, estimated as posterior modes. The corresponding posterior probabilities that  $\rho_{12}, \rho_{21}, \rho_{34}, \rho_{43}$  are equal to one are 1, 0.02, 0.11, 0.984 and 1, 1, 0.998, 1 before and during seizure, respectively.

When only using data from the left hemisphere, the inferred connections (namely, a unidirectional connection from Population 1 to 2 before seizure, and bidirectional connection during seizure) agree with those obtained in the 4-population-case. During the seizure period, the coupling strength  $L$  for the left hemisphere is slightly larger than for  $N = 4$  (grey versus blue lines in the top right panel of Figure 9a). Moreover, the coupling strengths of the left hemisphere seem to be larger than the right one, both before and during seizure. For the period prior to seizure, the inferred connections ( $\hat{\rho}_{34} = 0, \hat{\rho}_{43} = 1$ ) from the two populations on the right hemisphere (i.e., Population 3, FP2-F4, and Population 4, FP2-F8) also agree with the 4-population-case. However, this is not the case during seizure, as the bidirectional connections detected now for  $N = 2$  were not present when using data from all 4 channels, even if the coupling strength  $L$  and  $c$  assume smaller values than before (black vs blue lines in the top right panel and left bottom panel of Figure 9a).



(a)



(b)

Figure 9: **Estimation results for EEG recordings.** Three models are considered: Populations 1-4, modelling all four channels; Populations 1-2, modelling the left hemisphere; Populations 3-4, modelling the right hemisphere. (a) nSMC-ABC marginal posterior densities of the continuous parameters. Before seizure: solid green ( $N = 4$ ), dotted orange ( $N = 2$ , left hemisphere), dotted brown ( $N = 2$ , right hemisphere). During seizure: solid blue ( $N = 4$ ), dashed grey ( $N = 2$ , left hemisphere), dashed black ( $N = 2$ , right hemisphere). The solid red lines are the uniform prior distributions. (b) nSMC-ABC marginal posterior distributions of the discrete network parameters before seizure (top panels) and during seizure (bottom panels). The vertical dashed orange and red lines denote the estimated posterior modes for the reduced models with  $N = 2$  populations of the left and right hemispheres, respectively.



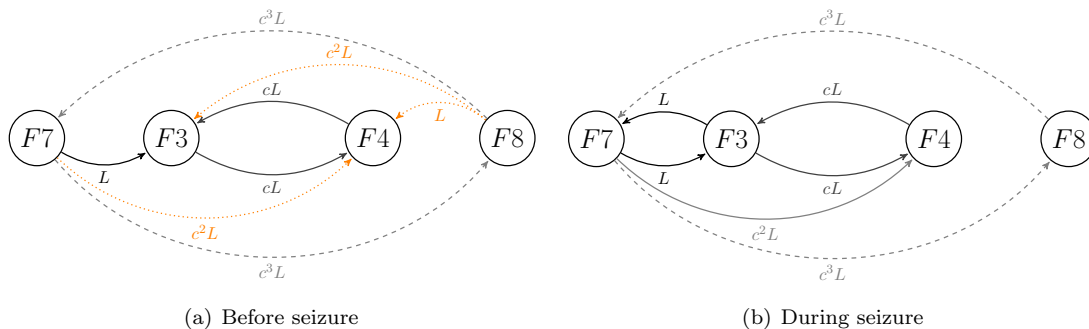


Figure 10: **Inferred network from EEG recordings.** Estimated network ( $N = 4$ , channels FP1-F7, FP1-F3, FP2-F4 and FP2-F8) for a 11 year old female patient before (a) and during (b) epileptic seizure. The dotted orange connections in (a) are estimated with a probability less than 0.75 (cf. top panels of Figure 9b).

**Fitted summaries** Figure 11 provides a comparison of the summary statistics (10) derived from the EEG recordings (solid black lines) and those obtained from datasets simulated under the 500 kept posterior samples of the 4-population model (grey regions). Median values of the summaries for the 2-population models of the left (dashed orange lines) and right (dashed red lines) hemispheres are also reported. The left and right panels of each subfigure correspond to the before and during seizure scenario, respectively. The match of the observed and simulated summaries is generally good, except for the MSCs, which are based on the cross-spectral densities. Moreover, the oscillations of the cross-correlation functions before seizure are not captured well, suggesting some lack of fit of the multi-population JR-NMM to the EEG data.

**Acceptance rate and runtime** In Figure 7b, we report the acceptance rate of particles and the runtime (in hours) of the 4-population-experiments as functions of the iteration  $r$  of the nSMC-ABC Algorithm 2 before (dotted red lines) and during (solid black lines) seizure. The acceptance rate dropped below the final threshold of 0.1%, causing the algorithm to terminate, after 59 and 72 iterations, respectively. The vertical lines indicate iteration 44 and 51, from which the network estimates (visualised in Figure 10) do not change anymore.

## 7 Conclusion and discussion

Understanding how different regions in the brain are connected and how they function together, e.g., during epileptic seizure, is a problem of large interest in the field of neuroscience. We contribute to this task by investigating a stochastic neural mass model, which describes the activity of multiple coupled neural populations in the brain. In particular, we extend the 1-population stochastic JR-NMM [1, 18] to a model of  $N$  coupled neural populations. This  $6N$ -dimensional SDE contains both a variety of continuous biologically motivated model parameters and  $\{0, 1\}$ -valued coupling direction parameters, which characterize the network structure among the  $N$  interacting populations. The goal is to estimate both types of parameters from  $N$  simultaneously observed time series datasets, corresponding to a multi-channel EEG recording. This task is particularly challenging, as none of the  $6N$  coordinates of the model is directly observed. Indeed, only the  $N$ -dimensional output (3), a multivariate linear function of the coordinates of the equation, is measurable with EEG recording techniques. Moreover, due to the intricacy of the model, the underlying likelihood function is not available.

We tackle these issues by extending the likelihood-free ABC method presented in [8] to the case of multiple interacting components. In particular, we consider the gold-standard SMC-ABC algorithm and adapt it to sample and perturb the continuous and binary parameter independently.

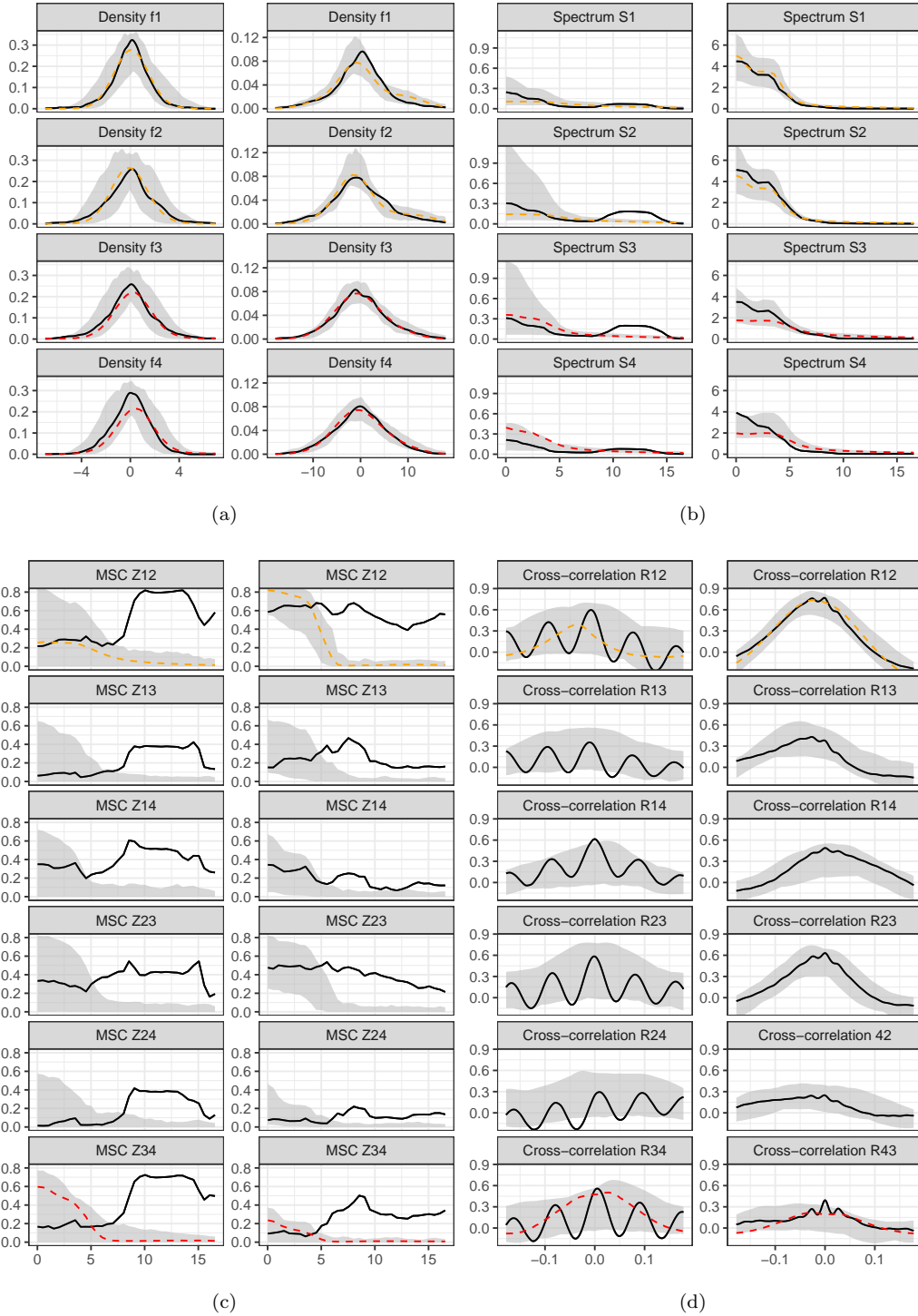


Figure 11: **Summaries from EEG recordings and the estimated traces.** Odd panels: before seizure; Even panels: during seizure. Solid black lines: Summaries derived from the EEG datasets visualised in Figure 8. Grey areas: Range of the summaries obtained from synthetic datasets simulated using the kept posterior samples from the full model with four channels ( $N = 4$ ). Dashed lines: Median values of the summaries derived from simulated datasets with  $N = 2$  populations for the left hemisphere (orange) and the right one (red).

The proposed nSMC-ABC algorithm requires two key ingredients: a reliable and computationally efficient numerical simulation method for data generation, and suitable summary statistics to compare the observed and simulated data, capturing the model dynamics and features independently of the underlying intrinsic stochasticity. First, we construct a numerical method to simulate from the model. The derived scheme is based on the splitting approach, it exploits the Hamiltonian structure of the model, and it is automatized for an arbitrary number of populations  $N$ . A standard integrator such as the Euler-Maruyama method would either lead to drastic fails in the estimation or make the algorithm computationally infeasible, as it would require a significantly smaller time discretisation step to capture the dynamics of the model (see [8] for an illustration of this issue on the stochastic JR-NMM with  $N = 1$ ). Second, we propose data summaries which take into account both individual signals as well as pairwise connectivity measures among signals. In particular, we map the  $N$ -dimensional time series to the  $N$  corresponding densities and spectral densities, and derive the  $N(N - 1)/2$  MSCs, which are based on the cross-spectral densities, and the  $N(N - 1)$  cross-correlation functions. These quantities are derived from a given dataset using standard estimators, e.g., a kernel density estimator and a smoothed periodogram estimator.

The resulting algorithm yields excellent estimation results when applied to simulated data in various scenarios, ranging from a cascade connectivity structure to a fully connected network of four populations. Applying the algorithm to real EEG data with epileptic activity yields a clear estimate of both the relevant continuous model parameters and the underlying network structure. Comparing the estimation results with those obtained from the data before seizure, we observe a larger activation in each of the individual neural populations, a larger noise intensity in both the left and the right brain hemisphere, a stronger connectivity in the left brain hemisphere, and a reduced one in the right brain hemisphere during seizure. The match of summary statistics derived from the experimental data and those generated using the weighted kept nSMC-ABC particles is generally good, except for the MSCs and the oscillations in the cross-correlations before seizure. This may be due to a lack of fit of the model, possibly due to the data not being Markovian, the chosen modelling of the coupling strength parameters or some of the underlying fixed parameters being slightly off.

The successful inference of the network parameters together with a relatively large number of continuous model parameters in the case of  $N = 4$  populations is remarkable, considering that previously, in the 1-population JR-NMM, only up to four continuous model parameters were simultaneously identified via ABC [8] or neural posterior estimation approaches [31]. Finally, we emphasise that the proposed nSMC-ABC algorithm, along with the presented summaries, can be directly applied to other coupled ergodic SDE models, as long as a suitable numerical simulation method for data generation is available. Moreover, the proposed methodology for network inference may be incorporated into more evolved ABC algorithms such as the guided sequential schemes introduced in [27], aiming to further reduce the overall inferential running times.

## References

- [1] M. Ableidinger, E. Buckwar, and H. Hinterleitner. A stochastic version of the Jansen and Rit neural mass model: analysis and numerics. *J. Math. Neurosci.*, 7(8), 2017.
- [2] L. Arnold. *Stochastic Differential Equations: Theory and Applications*. Wiley, New York, 1974.
- [3] M. A. Beaumont, J.-M. Cornuet, J.-M. Marin, and C. P. Robert. Adaptive approximate Bayesian computation. *Biometrika*, 96(4):983–990, 2009.
- [4] M. A. Beaumont, W. Zhang, and D. J. Balding. Approximate Bayesian computation in population genetics. *Genetics*, 162(4):2025–2035, 2002.
- [5] S. Blanes, F. Casas, and A. Murua. Splitting and composition methods in the numerical integration of differential equations. *Bol. Soc. Esp. Mat. Apl.*, 45, 2009.

- [6] S. Blanes, F. Diele, C. Marangi, and S. Ragni. Splitting and composition methods for explicit time dependence in separable dynamical systems. J. Comput. Appl. Math., 235(3):646–659, 2010.
- [7] E. Buckwar, A. Samson, M. Tamborrino, and I. Tubikanec. A splitting method for SDEs with locally Lipschitz drift: Illustration on the FitzHugh-Nagumo model. Appl. Numer. Math., 179:191–220, 2022.
- [8] E. Buckwar, M. Tamborrino, and I. Tubikanec. Spectral density-based and measure-preserving ABC for partially observed diffusion processes. An illustration on Hamiltonian SDEs. Stat. Comput., 30(3):627–648, 2020.
- [9] Z. Chen, B. Raman, and A. Stern. Structure-preserving numerical integrators for Hodgkin–Huxley-type systems. SIAM J. Sci. Comput., 42(1):B273–B298, 2020.
- [10] J. Chevallier, A. Melnykova, and I. Tubikanec. Diffusion approximation of multi-class Hawkes processes: Theoretical and numerical analysis. Adv. Appl. Probab., 53(3):716–756, 2021.
- [11] D. Cohen. On the numerical discretisation of stochastic oscillators. Math. Comput. Simul., 82(8):1478–1495, 2012.
- [12] J. M. Cornuet, F. Santos, M. Beaumont, C. P. Robert, J.-M. Marin, D. J. Balding, T. Guillemaud, and A. Estoup. Inferring population history with DIY ABC: A user-friendly approach to approximate Bayesian computation. Bioinformatics, 24(23):2713–2719, 2008.
- [13] P. Del Moral, A. Doucet, and A. Jasra. An adaptive sequential Monte Carlo method for approximate Bayesian computation. Stat. Comput., 22:1009–1020, 2012.
- [14] S. Ditlevsen and A. Samson. Hypocoelliptic diffusions: filtering and inference from complete and partial observations. J. Royal Stat. Soc. B, 81(2):361–384, 2019.
- [15] D. Eddelbuettel and R. François. Rcpp: Seamless R and C++ Integration. J. Stat. Soft., 40(8):1–18, 2011.
- [16] S. Filippi, P. B. Barnes, J. Cornebise, and M. P. H. Stumpf. On optimality of kernels for approximate Bayesian computation using sequential Monte Carlo. Stat. Appl. Genet. Mol. Biol., 12(1):87–107, 2013.
- [17] J. Foster, G. Reis, and C. Strange. High order splitting methods for SDEs satisfying a commutativity condition. arXiv, 2211.11884, 2022.
- [18] B. H. Jansen and V. G. Rit. Electroencephalogram and visual evoked potential generation in a mathematical model of coupled cortical columns. Biol. Cybern., 73(4):357–366, 1995.
- [19] B. H. Jansen, G. Zouridakis, and M. E. Brandt. A neurophysiologically-based mathematical model of flash visual evoked potentials. Biol. Cybern., 68:275–283, 1993.
- [20] C. Kelly and G. Lord. Adaptive time-stepping strategies for nonlinear stochastic systems. Ima. J. Numer. Anal., 38(3):1523–1549, 2017.
- [21] J. R. León and A. Samson. Hypocoelliptic stochastic FitzHugh-Nagumo neuronal model: mixing, up-crossing and estimation of the spike rate. Ann. Appl. Probab., 28(4):2243–2274, 2018.
- [22] X. Mao. Stochastic Differential Equations and Applications. Horwood Publications, Chichester, 1997.
- [23] J.-M. Marin, P. Pudlo, C. P. Robert, and R. Ryder. Approximate Bayesian computational methods. Stat. Comput., 22(6):1167–1180, 2012.
- [24] R. McLachlan and G. Quispel. Splitting methods. Acta Numer., 11:341–434, 2002.

- [25] A. Melnykova. Parametric inference for hypoelliptic ergodic diffusions with full observations. *Stat. Inference Stoch. Process.*, 23:595–635, 2020.
- [26] J. Østergaard, A. Rahbek, and S. Ditlevsen. Oscillating systems with cointegrated phase processes. *J. Math. Biol.*, 75:845–883, 2017.
- [27] U. Picchini and M. Tamborrino. Guided sequential abc schemes for intractable bayesian models. *arXiv*, 2206.12235, 2022.
- [28] P. Pilipovic, A. Samson, and S. Ditlevsen. Parameter estimation in nonlinear multivariate stochastic differential equations based on splitting schemes. *arXiv*, 2211.11884, 2022.
- [29] Y. Pokern, A. M. Stuart, and P. Wiberg. Parameter estimation for partially observed hypoelliptic diffusions. *J. Royal Stat. Soc. B*, 71(1):49–73, 2009.
- [30] R Development Core Team. *R: A Language and Environment for Statistical Computing*. R Foundation for Statistical Computing, Vienna, Austria, 2011.
- [31] P. Rodrigues, T. Moreau, G. Louppe, and A. Gramfort. Hnpe: Leveraging global parameters for neural posterior estimation. *NeurIPS*, 34, 2021.
- [32] M. G. Ruse, A. Samson, and S. Ditlevsen. Inference for biomedical data by using diffusion models with covariates and mixed effects. *J. R. Stat. Soc., C: Appl.*, 69(1):167–193, 10 2019.
- [33] A. H. Shoeb. Application of machine learning to epileptic seizure onset detection and treatment. *Dissertation, MIT Health Sciences and Technology Division*, 2009.
- [34] S. A. Sisson, Y. Fan, and M. Beaumont. *Handbook of Approximate Bayesian Computation*. Chapman & Hall/CRC Handbooks of Modern Statistical Methods. CRC Press, Taylor & Francis Group, 2018.
- [35] S. A. Sisson, Y. Fan, and M. M. Tanaka. Sequential Monte Carlo without likelihoods. *Proc. Natl. Acad. Sci. U S A*, 104(6):1760–1765, 2007.
- [36] G. Strang. On the construction and comparison of difference schemes. *SIAM J. Numer. Anal.*, 5(3):506–517, 1968.
- [37] A. H. Strømme Melbø and D. J. Higham. Numerical simulation of a linear stochastic oscillator with additive noise. *Appl. Numer. Math.*, 51(1):89–99, 2004.
- [38] S. Tiran and P. Maurine. SCA with Magnitude Squared Coherence. In S. Mangard, editor, *Smart Card Research and Advanced Applications*, pages 234–247, Berlin, Heidelberg, 2013. Springer Berlin Heidelberg.
- [39] T. Toni, D. Welch, N. Strelkowa, A. Ipsen, and M. P. H. Stumpf. Approximate Bayesian computation scheme for parameter inference and model selection in dynamical systems. *J. Roy. Soc. Interface*, 6(31):187–202, 2009.
- [40] H. F. Trotter. On the product of semi-groups of operators. *Proc. Am. Math. Soc.*, 10(4):545–551, 1959.
- [41] I. Tubikanec, M. Tamborrino, P. Lansky, and E. Buckwar. Qualitative properties of different numerical methods for the inhomogeneous geometric Brownian motion. *J. Comput. Appl. Math.*, 406:113951, 2022.
- [42] F. Wendling, J. J. Bellanger, F. Bartolomei, and P. Chauvel. Relevance of nonlinear lumped-parameter models in the analysis of depth-EEG epileptic signals. *Biol. Cybern.*, 83(4):367–378, 2000.